


ORIGINAL ARTICLE

Open Access



# Satellite constellation design for Titan exploration: orbit design and performance assessment

Lucas S. Ferreira<sup>1\*</sup> , Daniel Casanova<sup>2,4</sup>, Eva Tresaco<sup>3,4</sup> and Antonio F. B. A. Prado<sup>5</sup>

## Abstract

Satellite constellations allow distributed tasks among multiple spacecraft, reducing mission time and enhancing objectives. Interest in constellations has increased due to reduced costs in satellite production and launch. A key step in constellation planning is its design, which determines the orbital distribution of the satellites. In this work, we apply the 2D Necklace Flower Constellations methodology to explore possible architectures for future missions around Titan. As a result of strong perturbations in regions near natural satellites and environmental restrictions on Titan, proposals for maintaining constellations to enhance data collection and prevent mutual collisions between the satellites involved are an important aspect to consider. Therefore, the proposed designs incorporate frozen orbits and repetition ground tracks in an initial dynamical model that includes the effects of the  $J_2$  and  $J_3$  perturbations. Analyses using a simplified dynamic model, with a simple mean and a complete dynamic model, employing the IAS15 integrator from the Rebound package, show that, for the assumed perturbations, the proposed constellation configurations maintain long-term ground-track coverage of the surface of Titan. The performance evaluation indicates that the methodology provides robust constellation geometries, supporting orbit control and mission feasibility for Titan exploration.

**Keywords** Astrodynamics, Satellite constellation, Mission design, Necklace Flower Constellation, Titan

## Introduction

Small satellite constellations have received great interest in recent years. Factors motivating the implementation of these constellations include cost reductions in the production and launch of vehicles. As well as the

advantages associated with the functionalities of the satellites involved in the constellation. Compared to other missions, the primary operational objective of constellations is the possibility of distributing different targets among the vehicles involved, thus improving operations and possibly minimizing execution time. In addition, the various vehicles involved can be equipped with tools for alternative operations. In this way, satellites can be grouped or redirected to contribute to specific missions or replace the position of vehicles that may become inoperable due to various factors. An important part of planning constellations is the theory and methodology to be considered for formation and distribution of the satellites involved. Several studies have highlighted the challenges involved in managing the dynamics of multiple vehicles simultaneously (An et al., 2020; Li et al., 2023; Guo et al., 2023; Yang & Song, 2025).

\*Correspondence:

Lucas S. Ferreira  
ls.ferreira@unesp.br

<sup>1</sup> School of Natural Sciences and Engineering, São Paulo State University (UNESP), Rua Quirino de Andrade, 215, São Paulo 01049-010, Brazil

<sup>2</sup> Centro Universitario de la Defensa de Zaragoza, Academia General Militar, Crta. Huesca, s/n, 50090 Zaragoza, Spain

<sup>3</sup> Escuela Politécnica Superior, Universidad de Zaragoza, Crta. de Cuarte, s/n, 22071 Huesca, Spain

<sup>4</sup> IUMA, Universidad de Zaragoza, Pedro Cerbuna, 12, 50009 Zaragoza, Spain

<sup>5</sup> INPE, Postgraduate Division, National Institute for Space Research, Avenida dos Astronautas, 1.758, São José dos Campos 12227-010, Brazil



© The Author(s) 2025. **Open Access** This article is licensed under a Creative Commons Attribution 4.0 International License, which permits use, sharing, adaptation, distribution and reproduction in any medium or format, as long as you give appropriate credit to the original author(s) and the source, provide a link to the Creative Commons licence, and indicate if changes were made. The images or other third party material in this article are included in the article's Creative Commons licence, unless indicated otherwise in a credit line to the material. If material is not included in the article's Creative Commons licence and your intended use is not permitted by statutory regulation or exceeds the permitted use, you will need to obtain permission directly from the copyright holder. To view a copy of this licence, visit <http://creativecommons.org/licenses/by/4.0/>.

Over the years, many methodologies for possible projects have been proposed. Among the most well-known are Walker Constellations and Drain constellations, which focus on constellation designs involving polar and circular orbits and highly eccentric elliptical orbits, respectively. The Flower Constellations Theory was first introduced by Mortari et al. (2004), serving as the foundation for numerous studies over the years, such as The Lattice Flower Constellation, Avendaño et al. (2013), and Necklace Flower Constellation, Casanova et al. (2011), theories stand out, from which the 2D-Lattice Flower Constellation and 2D-Necklace Flower Constellation methodologies were developed (Avendaño et al., 2013; Arnas et al., 2018). Other works for 3D and 4D Lattice Flower Constellation and 3D-Necklace Flower Constellation have also been developed.

In addition to the development of possible designs for constellations, numerous studies have explored orbital configurations for spacecraft around planets and their natural satellites. In this context, studies focusing on orbits with properties such as trajectory repetition, frozen orbits, spin-orbit resonance, among others, are being investigated and encouraged (Elipé & Lara, 2003; Tresaco et al., 2016; Formiga & Moraes, 2011). Given that many of these spacecrafts are intended to operate closer to the surface of these celestial bodies, scenarios with the presence of perturbative forces due to the non-uniformity of the natural satellite's mass, among others, have been realized and encouraged.

The moons of Saturn are among the most intriguing celestial bodies in our solar system, each exhibiting unique characteristics that have attracted significant scientific interest. Research on these moons includes various fields, including geology, atmospheric science, and astrobiology, offering insights into their formation, evolution, and potential for hosting life.

Titan, Saturn's largest natural satellite, is notable for its thick atmosphere and liquid hydrocarbon lakes. Studies have revealed that Titan's atmosphere is rich in nitrogen, with a complex organic chemistry that may provide clues about prebiotic conditions similar to those on early Earth. The Cassini-Huygens mission provided extensive data on Titan's surface and atmospheric dynamics, leading to the discovery of rain, rivers, and lakes composed of methane and ethane. Future missions, such as the Dragonfly mission, aim to explore Titan's diverse environments and their potential for life.

Enceladus has emerged as a key target in the search for extraterrestrial life due to its active geysers, which eject water vapor and organic materials from its subsurface ocean into space. The Cassini spacecraft made significant discoveries regarding the moon's plumes, revealing that they contain salts and organic compounds, suggesting

a chemically active interior conducive to life. Ongoing studies aim to analyze the composition of these plumes and understand the moon's geophysical processes (Peter et al., 2024).

Therefore, research on the moons of Saturn has transformed our understanding of these distant worlds, revealing complex geological processes and environments that may harbor life. Continued exploration, particularly through upcoming missions, promises to deepen our insights into the potential habitability of these fascinating celestial bodies.

In particular, due to its atmospheric composition, its active methane cycle, and the constant chemical interaction between its surface and atmosphere, the natural satellite Titan can be found as a potential target for future exploration missions (Lunine, 1997; Hörst, 2017; Lopes et al., 2020).

In conjunction with the diversity of interests and motivational aspects in the most diverse areas for the exploration of the natural satellite Titan, see section "[Mission requirements](#)" for more. This natural satellite presents interesting challenges related to the allocation of spacecraft and, consequently, satellite constellations. Although it is the largest natural satellite of Saturn, the perturbing effects of the planet are still an object of investigation, thus promoting that the orbital planes around this natural satellite should be present in the regions closest to the natural satellite and its region of gravitational dominance. Although in the case of Titan, its gravitational influence causes this region to be slightly larger than for satellites with lesser gravitational influences. In addition to these restrictions, Titan's gravitational configuration and the influence of its harmonic perturbations, due to its non-uniform mass distribution, more strongly in zonal perturbations, followed by sectorial ones, make the design and maintenance of satellite constellations a more complex process (Turtle et al., 2018; Ferreira et al., 2022). The distance of this natural satellite, as well as the amount of sunlight received, are also important constraints in the development of constellations, since systems using solar energy and information transmission are more challenging. Thus motivating the implementation of constellations with satellites that are more autonomous and with high predictability and periodicity in their orbital evolutions. Another interesting factor is Titan's well-known atmosphere. For satellites to be placed at a safe orbital distance, they must be at an altitude of over 1,500 km to avoid the effects of atmospheric drag (Hörst, 2017). Furthermore, due to its dense atmosphere, composed of a thick layer of hydrocarbon haze, it is known that this configuration tends to make it difficult to obtain high-resolution images due to light scattering and absorption (Hörst, 2017; Rianço-Silva et al., 2024; Gopalchetty

& Coates, 2025). Thus, previous missions and studies (Barnes et al., 2007; Wye et al., 2007) highlight specific wavelengths as well as the use of radiometry and other tools and methods for obtaining and collecting data. In this context, observations of Titan must be aligned with atmospheric transmission windows (Barnes et al., 2020). Similarly as studies of Earth-related satellite navigation have been seeking proposals to address the challenges present in the Earth's atmospheric layers (Li et al., 2020; Hein, 2020). These aspects are directly related to the field of satellite navigation, since accurate determination of orbits, control strategies, distribution, and performance evaluation are essential to ensure the viability of the mission. Thus, the overall objective of this study is to explore robust constellation architectures for the exploration of Titan using the Flower Constellations methodology. More specifically, this work presents a novel approach to the design of satellite constellations around Titan by combining advanced theoretical frameworks and practical orbital strategies. Specifically, it leverages the 2D-Necklace Flower Constellation methodology to systematically arrange multiple satellites while ensuring uniform coverage and efficient phasing. The advantages provided by the 2D-Necklace Flower Constellation methodology, a model derived from the Necklace Flower Constellation (Casanova et al., 2011) and the Flower Constellation methodology (Mortari et al., 2004), include the fact that its structure allows for various design possibilities based on parameters such as relative phasing, orbital spacing, and repetition of ground tracks, while maintaining symmetry and coverage properties (Casanova et al., 2014; Arnas et al., 2018). Among the possible models are classic designs such as Walker and Walker delta (mixed) constellations (Walker, 1984). Thus, the 2D-Necklace Flower Constellation methodology is a general framework that inherently encompasses classical designs as particular cases (Arnas et al., 2017a, b). Because it is not traditionally limited to Earth-based applications, it thus offers advantages in terms of generality and adaptability to specific mission constraints, such as those encountered in the exploration of Titan.

In addition, the proposed constellations are based on orbits with repeating ground tracks and frozen orbit characteristics, which are particularly advantageous for long-duration missions in perturbed environments such as Titan's gravitational field. These choices allow for sustained observational capabilities over specific regions of interest, reduced station-keeping requirements, and improved mission resilience. This integrated approach represents a significant advancement over conventional constellation architectures and is especially suited to the unique challenges posed by Titan's orbital dynamics and scientific exploration needs. So the constellations

designed in this paper through the presented methodology demonstrates efficiency over other methods, reducing the needed number of satellites or increasing the coverage. In general, as a starting point for research on constellations around natural satellites, we proposed a study of the natural satellite Titan to investigate theoretical orbits assuming simplified dynamic conditions. Initially, we highlight only the gravitational effects of Titan and, due to its harmonics, those related to the asymmetries of its poles. With this approach, we seek to consolidate the methodology subject to these conditions and evaluate the dynamics in view of the analysis of the impact of the satellites present in these constellations. The aim is to evaluate the performance of the methodology and navigation proposed for the satellites under investigation. Promoting analyses for the improvement of the methodology and new maintenance proposals. In this respect, by addressing these issues, this work contributes to bridging the gap between constellation theory and its application to planetary satellite navigation. Assessments of the stability, coverage, and sensitivity to disturbances of the constellations also motivate potential applications for future investigations.

### Constellation theory

In recent decades, satellite cooperation has become central to space missions, especially in telecommunication, observation, and reconnaissance missions. These missions use constellations of similar satellites to ensure continuous or discontinuous coverage. Various constellation designs have appeared, such as Walker Constellations, Streets of Coverage, Drim Constellations, and Flower Constellations. However, most of these constellation designs make assumptions that limit their direct application. To overcome some of these limitations, Lattice and Necklace Flower Constellations were introduced as a generalization of Flower Constellations. In this work, we focus on the design methodology of 2D Lattice and Necklace Flower Constellations for different missions to explore Titan.

In consequence, in this section, we will focus on the Flower Constellation Theory, the 2D Lattice Flower Constellation, and 2D Necklace Flower Constellation methodologies, which will be the main methodology used in this investigation. Subsequently, we will present the motivations and regions of interest in the natural satellite Titan, highlighting the requirements and restrictions imposed to perform the mission and the planning of the constellation designs. Next, the criteria and methodologies used to obtain the orbital elements for constructing the nominal orbits that will form the constellations will be presented.

### Flower constellations theory

Initially presented in the works of Mortari et al. (2004). The theory of Flower Constellations is known for using knowledge of Number Theory. In general, this design model has the characteristic that, given a set of satellites, it generates orbital conditions that allow all the vehicles involved in the dynamics to have the same trajectory, considering a rotating reference system fixed to the central body. In this way, previous works, Mortari and Wilkins (2008), highlight that this property is obtained by determining that the trajectories are generated considering compatible or resonant orbits concerning the different rotating references that can be adopted and that share a commensurability between their angular velocities. The conditions of the Flower Constellation Theory can be generalized into three general conditions. Initially, to ensure that the trajectory in the rotating reference system is closed and three-dimensional, the commensurability condition in Eq. (1) should be guaranteed.

$$N_p T_p = N_d T_d. \quad (1)$$

The values  $N_p$  and  $N_d$  are integers and represent the number of orbital periods of satellites and the number of sidereal days it takes to repeat the ground-tracker (Mortari et al., 2004). The value  $N_p$  also represents the number of petals, which gives the Theory its name. The other parameters  $T_p$  and  $T_d$  correspond to the period of revolution of each satellite and revolution of the central body, respectively. Concerning the orbital elements, the orbits that compose the constellation must have the same values for the orbital elements inclination ( $I$ ), semi-major axis ( $a$ ), argument of the pericenter ( $\omega$ ), and eccentricity ( $e$ ), and the eccentricity of the orbit is not restricted to circular cases (Mortari & Wilkins, 2008; Avendaño et al., 2013). The distribution of the satellites in this model is done by distributing the values of the mean anomaly  $M_{ij}$  and the longitude of the ascending node  $\Omega_{ij}$  of each satellite that makes up the constellation based on Mortari and Wilkins (2008), by Eq. (2), to maintain uniformity in the distribution considering the various orbital planes.

$$N_p \Delta\Omega_{ij} + N_d \Delta M_{ij} = 0 \pmod{2\pi}. \quad (2)$$

These conditions are necessary and sufficient for all the satellites involved in the constellation to have the same trajectory in the rotating reference system. The expressions for the values of the ascending node longitude and mean anomaly elements for the Flower Constellations model are well known and are available in the works of Mortari and Wilkins (2008).

#### 2D Lattice Flower Constellation.

Derived from the Theory of Flower Constellations is the design methodology known as 2D Lattice Flower

Constellation (2D-LFC) (Avendaño et al., 2013; Arnas et al., 2018). Having nine parameters as its basis, the 2D-LFC maintains the characteristic that all the orbits that form the constellation have the same nominal values for the orbital elements inclination ( $I$ ), eccentricity ( $e$ ), semi-major axis ( $a$ ) and the argument of the pericenter ( $\omega$ ). The other orbital elements, the longitude of the ascending node ( $\Omega_{ij}$ ) and the mean anomaly ( $M_{ij}$ ), in each orbit, are established utilizing the possible combinations generated and arranged in the phase space ( $\Omega, M$ )-space. As stated in the name of the methodology, the points arranged in the phase space have the appearance of a network, since the model always seeks to maintain the characteristics of symmetry and uniformity in the distributions of the orbits and orbital planes. Therefore, six parameters considered in 2D-LFC are related to the shape and distribution of the orbits that compose the constellation. The other parameters, known as  $N_\Omega$ ,  $N_M$  and  $N_{M\Omega}$ , are related to the configurations of the design, being the number of orbits, the number of satellites per orbit and the phasing coefficient of the constellation distributions, respectively.

Taking into account the knowledge related to number theory and modular arithmetic, Avendaño et al. (2013) showed that the possible combinations of values for the longitude of node and the mean anomaly of each satellite in the constellation can be obtained by considering the solutions of Eq. (3) in Hermite Normal form. These values can also be arranged in a phase space ( $\Omega, M$ )-space, whose distribution of points resembles a lattice, which is related to the name of the design.

$$\begin{pmatrix} L_\Omega & 0 \\ N_{M\Omega} & N_M \end{pmatrix} \begin{pmatrix} \Delta\Omega_{ij} \\ \Delta M_{ij} \end{pmatrix} = 2\pi \begin{pmatrix} i-1 \\ j-1 \end{pmatrix}. \quad (3)$$

Considering that the indices  $i$  and  $j$  correspond, respectively, to the orbit to which the satellite belongs and its position within the orbit, Eq. (3) is valid in the range  $1 \leq i \leq N_\Omega$  and  $1 \leq j \leq N_M$ . The orbit phasing parameter assumes a range of possible values taking into account the number of orbital planes in the interval  $0 \leq N_{M\Omega} \leq (N_\Omega - 1)$ . The quantities  $\Delta\Omega_{ij}$  and  $\Delta M_{ij}$  correspond to the variation in the longitude of the ascending node and the value of the mean anomaly based on an initial reference satellite with the notation  $\Delta\Omega_{11}$  and  $\Delta M_{11}$ .

### Necklace Flower Constellations Theory

Although the 2D Lattice Flower Constellations model can be used in various approaches, it is known that it has some limitations related to the total number of different designs that can be generated. This limitation is linked to the characteristics that maintain the homogeneity and symmetry of the distributions, since in



the 2D-LFC model the positions generated must all be occupied by the satellites involved in the constellation. Therefore, by considering the  $(\Omega, M)$ -space as a mesh, the model guarantees that each node in the mesh must be occupied by a vehicle.

In terms of the parameters involved in the design, it is known that the number of orbital planes  $N_\Omega$  and the number of satellites per orbit  $N_M$  are fixed by the design, so the parameter responsible for generating phasing, and thus different designs, is the parameter  $N_{M\Omega}$ .

Since this parameter is related to the number of orbital planes, in order to have more different designs, it is necessary to have a larger number of satellites involved in the dynamics and/or a larger number of orbital planes (Arnas et al., 2018). Although this condition is favorable when considering constellations made up of large numbers of satellites, the model presents restrictions when designing missions aimed at constellations with small numbers of vehicles, to maximize the performance of the spacecraft involved.

In response to this question and with the aim of contributing to research related to constellation design, Casanova et al. (2014) present a new design methodology using a strategy to maximize the number of possible distinct configurations, based on the Theory of Necklaces. Considering an orbit of the constellation, if we define  $N_{fso}$  as the total number of fictitious positions on the orbit and  $N_{rso}$  as the real number of satellites, where  $N_{rso} \leq N_{fso}$ , the model aims to determine the total number of possible subsets (sub-constellations) within a fictitious set (fictitious constellation). When adjusted to a physical problem associated with orbital dynamics, the theory of necklaces was restricted to a system with only two possibilities, where solutions can be obtained motivated by Casanova et al. (2011).

Thus, considering  $n$  admissible positions for the satellite, the mathematical notation  $\mathcal{G} = \{1, 2, \dots, n\}$  is presented as the algebraic representation of a necklace, with the positions occupied by the satellites indicated by the indices. An important definition related to the theory is the idea of identical necklaces. If  $r$  is taken as an integer, identical necklaces are those that satisfy Eq. (4). In this way, identical subsets are those that can be returned through  $r$  rotations.

$$\mathcal{G}_i \approx \mathcal{G}_j \Leftrightarrow \mathcal{G}_i = \mathcal{G}_j + r \pmod{n}. \quad (4)$$

Related to the uniformity of the distribution of necklaces, Casanova et al. (2011) presents the concept of symmetry ( $Sym(\mathcal{G}_i)$ ). Defined by Eq. (5), given an initial necklace  $\mathcal{G}_i$ , the integer value of the symmetry is obtained by counting the minimum number of rotations necessary for the configurations obtained to be identical.

$$Sym(\mathcal{G}_i) = \min \{1 \leq r \leq n : \mathcal{G}_i + r \equiv \mathcal{G}_i \pmod{n}\}. \quad (5)$$

Considering the previous definitions, the 2D Necklace Flower Constellations model can be formalized by considering all the admissible subsets of necklaces and by incorporating them into the equations that determine the possible pairs of phase space  $(\Omega, M)$ -space of the 2D Lattice Flower Constellations model. To do this, assuming  $N_0$  as the number of orbital planes,  $N_c$  as the phasing coefficient and keeping the parameters  $N_{fso}$ ,  $N_{rso}$  and  $Sym(\mathcal{G})$  already established, it is possible to compute all possible subsets of necklaces, as well as to obtain a new shifting parameter,  $k$ , with domain in the interval  $1 \leq k \leq (Sym(\mathcal{G}) - 1)$  determined by Eq. (6), which aims to determine the set of parameters that define a design whose relative constellation geometry is invariant with respect to the orbital plane or the moment of observation (Arnas et al., 2018).

$$Sym(\mathcal{G}) \mid kN_o - N_c. \quad (6)$$

Therefore, Eqs. (7)–(8) contain the expressions that determine the values of the orbital elements longitude of the ascending node  $\Omega_{ij}$  and mean anomaly  $M_{ij}$  for the 2D - Necklace Flower Constellation model.

$$\Omega_{ij} = \frac{2\pi}{N_o}(i-1) + \Omega_{11}, \quad (7)$$

$$M_{ij} = \frac{2\pi}{N_{fso}}(i-1)\gamma - \frac{2\pi}{N_{fso}} \frac{N_c}{N_o}(i-1) + M_{11}, \quad (8)$$

where  $M_{11}$  is the mean anomaly of the first satellite of the first orbit and,  $\gamma = \text{mod}(\mathcal{G}_M(j) - 1 + N_c(i-1), Sym(\mathcal{G}_M))$ .

After obtaining the pairs  $(\Omega, M)$ -space the other orbital elements, inclination ( $I$ ), eccentricity ( $e$ ), semi-major axis ( $a$ ) and the argument of the pericenter ( $\omega$ ) can be determined depending on the criteria chosen for the missions or the restrictions required for orbit. Following previous works (Arnas et al., 2021), to locate satellites from different orbital planes in the same ground-track, must be fulfilled:

$$N_d N_c + A N_o N_{fso} = N_p N_{fso}, \quad (9)$$

where  $A$  represents an unknown integer number. For a deeper understanding of this equation and some application cases see Ref. Arnas et al. (2018). In the next section, some characteristics of the natural satellite Titan, the target body of this work, will be presented. Some main points of interest in studying this natural satellite are also presented, as well as the criteria for future missions to these regions.

## Design requirements

In this section, two main aspects of the design requirements are addressed. On the one hand, mission requirements are analyzed, as they determine the specific needs and constraints based on mission objectives. On the other hand, the section explores different orbital properties, such as repeat-groundtrack or frozen orbits, which play a crucial role in the mission design. These aspects will be further developed in the following subsections.

## Mission requirements

Titan is the largest natural satellite of Saturn and the second-largest natural satellite in the Solar System. It is a celestial body full of characteristics that arouse the interest of researchers from the most diverse fields of knowledge. Given its similarities to processes that occur on Earth, this natural satellite is one of the candidates for future space exploration missions (Lorenz et al., 2018).

Among these characteristics, there is its dense, nitrogen-rich atmosphere, with an active methane cycle that actively and constantly influences the dynamics and atmospheric composition of the natural satellite (Hörst, 2017).

Being the only other body with a thick nitrogen ( $N_2$ ) atmosphere besides Earth, its atmospheric activities also influence the climate dynamics of natural satellite since its chemical composition is responsible for contributing to a greenhouse effect present on Titan (Hörst, 2017). The atmosphere of Titan is also notable for actively contributing to the composition and relief of the surface of the natural satellite. This interaction has a unique characteristic in our system, as the materials produced by atmospheric chemistry are transported or deposited, through wind and river processes, in the most diverse regions of the natural satellite's surface. This means that the surface of Titan is constantly changing atmosphere-surface.

Previous work (Lunine, 1997) shows that this integration affects the formation of the extensive dune fields, lakes, and seas present on Titan. Research on the natural satellite, Lopes et al. (2013), also highlights the modifications to the surface of Titan by various processes such as cryovolcanism, dissolution, and precipitation, as well as erosive processes and impact-generated craters. Due to its distance from the Sun, the natural satellite also has a complex methane cycle, which plays a role similar to that of water on Earth. This currently makes Titan one of the few bodies in the Solar System with stable liquid on its surface. This cycle is responsible for the formation of the entire hydrological process present on the natural satellite.

Given the various motivational points for exploring Titan, the geological map in Fig. 1 was taken from the work of Lopes et al. (2020). By studying radar and

infrared data provided by the Cassini mission, they cataloged the surface of Titan into 6 main units: hydrological regions composed of lakes and seas, in blue; crater regions, in dark green; dunes, in lilac; or plains, in light green. And two regions are classified as labyrinth regions, in pink, and hummocky, in orange.

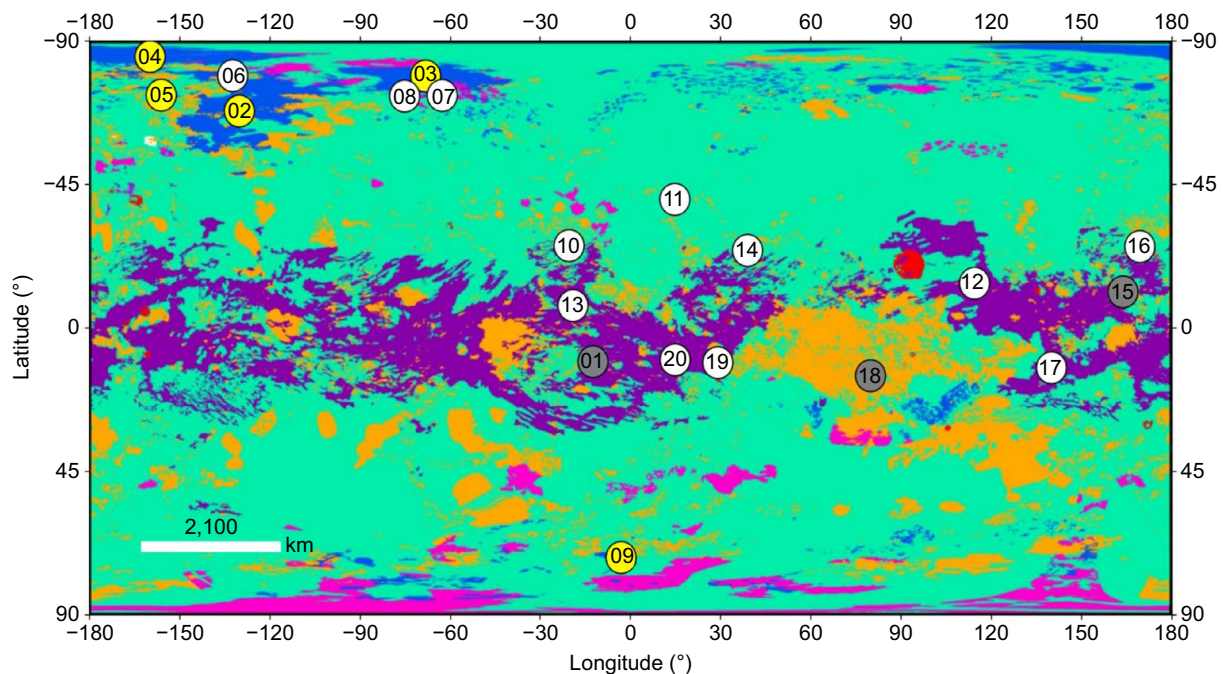
In general, Lopes et al. (2020) presented that the geological formations of Titan are mainly distributed latitudinally. Being predominantly composed of plains, approximately 65% of the total surface area, the plains present on Titan are found in greater proportion in the mid-latitude regions and also close to the equator. This is the region where dune formations are most prevalent. Due to the strong atmosphere-surface interactions, in these regions, it is possible to find regions with very similar organic compositions. Corresponding to the second largest geological unit on Titan, these dunes are found in the most equatorial and low-latitude regions, with an amplitude of no more than 30 degrees. The studies also classify regions with labyrinthine and hummocky units, which correspond, respectively, to plateau-like regions and mountainous regions in isolated terrain.

In contrast to the other regions, the lakes and labyrinths present on Titan are more dominant formations of the polar regions. Its hydric regions correspond to less than 2% of the surface of the natural satellite. To the north are most of the lakes and seas, such as Kraken Mare, Ligeia Mare, and Punga. And to the south by Ontario Lacus. Composed of several lakes, many works divide these units into dry and full regions. Several liquid hydrocarbon structures are found in these lakes (Poggiali et al., 2024). Given the high activity of the satellite, studies show that the youngest units are the lakes and dunes. Crater regions are also found on Titan, although to a lesser extent.

Because of the characteristics and potential of Titan, this natural satellite is among the bodies in potential research aimed at studying the origin of life and habitability.

In this work, we aim to contribute to the research by seeking configurations for the constellation of satellites around Titan. As a criterion required for the formation, we sought to determine sites of interest that can be used as reference regions. Figure 1 shows the location of 20 sites of interest on the surface of the natural satellite Titan.

These sites include regions of lakes and seas, as well as the main regions of dunes, craters, and Hummocky. In this paper, we have highlighted subgroups, with Titan's major lake and seas regions highlighted in yellow, as observation targets for the proposed Constellation Titan I mission. Meanwhile, the Huygens descent site, the central Xanadu region, and Sinlap are marked



[01] Huygens Landing (-12.335°, -10.573°) [02] Kraken Mare (-130°, 68°) [03] Ligeia Mare (-68°, 79°) [04] Punga Mare (-159.7°, 85.1°)  
[05] Jingpo Lacus (-156°, 73.0°) [06] Mayda Insula (-132.2°, 79.1°) [07] Vid Flumina (-62.5°, 72.9°) [08] Kokytos Flumina (-75.0°, 72.71°)  
[09] Ontario Lacus (-3°, -72.0°) [10] Afekan (-20.3°, 25.8°) [11] Hano (14.9°, 40.3°) [12] Ksa (114.6°, 14.0°)  
[13] Selk (-19.0°, 7.0°) [14] Soi (39.1°, 24.3°) [15] Sinlap (164.0°, 11.3°) [16] Forseti (169.6°, 25.5°)  
[17] Sotra Patera (140.2°, -12.5°) [18] Xanadu (80.0°, -15.0°) [19] Guabonito (29.2°, -10.9°) [20] Shangri-La (15.0°, -10.0°)

**Fig. 1** Location of points of interest on the surface of the natural satellite Titan. The yellow points correspond to Constellation Titan I, highlighting the points with Titan's main lakes and seas. The gray points correspond to Constellation Titan II, highlighting three more equatorial points of interest. Geological map taken from Lopes et al. (2020)

**Table 1** Values of the harmonic coefficients of Titan, Saturn's natural satellite

Harmonic	$\times 10^{-6}$
$J_2$	$33.089 \pm 0.609$
$J_3$	$-0.179 \pm 0.720$
$J_4$	$-1.077 \pm 1.844$
$C_{22}$	$10.385 \pm 0.084$

in gray as targets for the proposed Constellation Titan II mission. The latitude and longitude coordinates of each point are given in the legend below the geological map in Fig. 1. The points selected for Constellation Titan I correspond to regions of the Kraken Mare, Ligeia Mare, and Punga Mare seas, and the two largest lakes Jingpo Lacus and Ontario Lacus.

Considering the mass inhomogeneity of the natural satellite, Table 1 presents the values for some of the harmonic coefficients used in this work.

### Orbital requirements

When planning space missions, one of the important stages in the design process is planning the orbits that form the constellation. Given this, the stability of these orbits must be taken into account in order, among other things, to minimize costs related to burning fuel and carrying out corrective maneuvers (Cornara et al., 2001; Pontani et al., 2022). These are important aspects because they aim to keep the constellation design more stable, thus promoting the performance of the constellation and its related operations for as long as possible. Given these aspects, frozen orbits can be one of the strategies used (Delsate et al., 2010; Ovchinnikov et al., 2024).

Allied to the idea of stability and predictability, orbits that have the property of promoting multiple crossings over specific points on the surface of the orbited body with a certain regularity are also important conditions to be considered when planning constellations.

Thus, this study aims to determine orbital conditions characterized by these combined properties. In relation to the Titan natural satellite, based on previous work (Lorenz et al., 2008; Lopes et al., 2020), it is known that several regions of interest on the natural satellite are



close to polar or equatorial regions. It is known that the effects due to the non-sphericity of the central body tend to disturb these orbits. We are looking for conditions that promote shared trajectories in the relative system and that are frozen orbits, considering some of these perturbations. As an initial model, we consider, more precisely, the zonal perturbations  $J_2$  and  $J_3$  of Titan, given in Table 1.

#### Frozen Orbits Property

Presented by previous works as Lara et al. (1995); Elipse and Lara (2003); Abad et al. (2009), frozen orbits have the characteristic of maintaining, through an averaged system, some of their orbital elements constant during their orbital trajectory.

Frozen orbits are designed to maintain a nearly constant altitude relative to specific surface points of the orbited body. This stability is achieved by carefully selecting the orbital parameters, particularly the eccentricity ( $e$ ) and the argument of pericenter ( $\omega$ ), to minimize long-term variations. By ensuring that the rates of change of these parameters remain close to zero on average, frozen orbits prevent orbital drift, allowing spacecraft to follow a more stable trajectory without continuous corrections (Liu et al., 2011).

This favors missions related to observation and mapping. In addition, these conditions tend to contribute to obtaining long-duration orbits because, by keeping the eccentricity and argument of the pericenter more stable, they can reduce the effects that lead orbits to become more eccentric, taking the pericenter of the orbit to regions internal to the orbited body, thus promoting the loss of spacecraft by collision (De Almeida Prado, 2003; Cinelli et al., 2022).

The dynamic model assumed in this work considers the effects due to the non-uniformity of the mass resulting from the zonal harmonics  $J_2$  and  $J_3$ . Thus, the disturbance potential, based on Tresaco et al. (2016, 2018), can be written in the form:

$$R_{J_2J_3} = -\frac{\mu R_T^2 (3J_2 r s_i^2 \sin^2(\theta) - J_2 r)}{2r^4} - \frac{\mu R_T^2 (5J_3 R_T s_i^3 \sin^3(\theta) - 3J_3 R_T s_i \sin(\theta))}{2r^4}, \quad (10)$$

where  $R_T$  is the equatorial radius of the natural satellite,  $s_i = \sin i$ ,  $\theta = \omega + f$ , and  $f$  is the true anomaly.

Considering the potential of Eq. (10), based on Paulo dos Santos Carvalho et al. (2013), the frozen conditions can be obtained by reducing the number of degrees of freedom of the system when eliminating the terms related to the short-period perturbations of the perturbing potential. To do this, the movement of the spacecraft must be considered on an averaged model. In this way, we will analyze the

general perturbative effects resulting from each period of the spacecraft around the central body.

Thus, given a perturbation function  $F$ , we can define the average of this function, based on Tresaco et al. (2016) by Eq.(11), which determines the average over the mean anomaly:

$$\langle F \rangle = \frac{1}{2\pi} \int_0^{2\pi} F dM. \quad (11)$$

Since the relations between the mean anomaly  $M$ , the true anomaly  $f$ , and the eccentric anomaly  $E$  are known, the potential Eq. (10) is averaged over the mean anomaly. Thus, Eq. (12) is obtained:

$$\langle R_{J_2J_3} \rangle = \frac{J_2 n^2 R_T^2 (3 \cos(2i) + 1)}{8(1 - e^2)^{3/2}} - \frac{3e J_3 n^2 R_T^3 \sin(i) (5 \sin^2(i) - 4) \sin(\omega)}{8a(e^2 - 1)^{5/2}}. \quad (12)$$

Considering the average potential obtained in Eq. (12), the expressions for the rates of variations of the eccentricity and the argument of the pericenter can be obtained by introducing the potential into Lagrange's planetary equations, Eq. (14) (Vallado, 2001).

$$\frac{de}{dt} = \frac{\sqrt{1 - e^2}}{na^2 e} \frac{\partial R}{\partial \omega} - \frac{1 - e^2}{na^2 e} \frac{\partial R}{\partial M}, \quad (13)$$

$$\frac{d\omega}{dt} = -\frac{\sqrt{1 - e^2}}{na^2 e} \frac{\partial R}{\partial e} + \frac{\cot(i)}{na^2 \sqrt{1 - e^2}} \frac{\partial R}{\partial i}, \quad (14)$$

where  $R = \langle R_{J_2J_3} \rangle$ .

Consequently, the expressions for the rates of variation  $\frac{de}{dt}$  and  $\frac{d\omega}{dt}$  can be obtained considering the perturbation forces from coefficient  $J_2$  and  $J_3$ .

$$\frac{de}{dt} = \frac{3J_3 R_T^3 \sqrt{\mu} \sin(i) (5 \cos(2i) + 3) \cos(\omega)}{16a^{9/2} (1 - e^2)^2}. \quad (15)$$

$$\frac{d\omega}{dt} = \frac{3\mu^{1/2} R_T^2 (\alpha + \beta)}{64a^{9/2} e (1 - e^2)^3}, \quad (16)$$

where,

$$\alpha = 8ae(e^2 - 1)J_2(5 \cos(2i) + 3),$$

$$\beta = J_3 R_T \csc(i) \sin(\omega) \left( (35e^2 + 5) \cos(4i) - 3e^2 - 4 \cos(2i) - 1 \right).$$



Based on Eqs. (15)–(16), the conditions that guarantee frozen orbits can be obtained by imposing the condition of Eq. 17 and performing the necessary calculations.

$$\frac{de}{dt} = 0, \quad \frac{d\omega}{dt} = 0. \quad (17)$$

The first equation holds when  $\cos \omega = 0$ , that is, for  $\omega = \pi/2$  or  $3\pi/2$ ; thus, by replacing these values into the second equation of Eq. (17), its solution results in a surface parametrized by the orbital elements ( $a, e, i$ ).

#### Repeating ground-track property

The repeating ground track is another interesting property when it involves orbits for the purpose of allocation of spacecrafts to missions with various operations. These orbits are related to the regularity of vehicle overflights over specific regions of the surface of the body of interest. Some of its main applications are related to studies on the effects of the non-uniformity of the gravitational field, atmospheric and climatic effects, as well as remote sensing, data collection, and data transmission (Circi et al., 2014; Nadoushan & Assadian, 2015).

In general, this property can be applied to the orbits of interest by obtaining semi-major axis that maintain the commensurability relation between the number of orbital periods of the vehicle,  $N_p$ , and the number of days until the repeat passage over the region of interest,  $N_d$ . With  $N_p$  and  $N_d$  being two integer values,  $T_p$  being the orbital period of the probe and  $T$  being the rotation period of the orbiting body, in the absence of dissipative forces. The condition for repeating the trajectory is given by Eq. (18).

$$N_p T_p = N_d T. \quad (18)$$

Given the definition of the orbital period, we can find an initial expression to obtain the value of the semi-major axis of the orbit of spacecraft that maintains the required property.

$$a = \mu^{1/3} \left( \frac{TN_d}{2\pi N_p} \right)^{2/3}, \quad (19)$$

where  $\mu$  is the mass ratio of the natural satellite.

Because of the disturbances involved in the space environment, but precisely the disturbances related to the harmonic coefficients due to the proximity of the orbits of spacecraft of celestial bodies, the term due to the rate of change in the longitude of the ascending node has to be taken into account (Vallado, 2001).

The nodal period, which determines the time between two node line crossing events, must also be considered in the commensurability relation. Taking its definition and the definition of the rotational period of the central body, the commensurability expression (Wertz, 2002) can be written in the form of Eq. (20):

$$\frac{N_d}{N_p} = \frac{\theta - \dot{\Omega}}{\dot{\omega} + \dot{M}}. \quad (20)$$

Where  $\theta$  is the angular velocity of the orbiting body and  $\dot{\Omega}$ ,  $\dot{\omega}$  and  $\dot{M}$  are the rates of variation of the orbital elements.

Initially considering only the variations from the perturbative effects arising from the zonal harmonic  $J_2$ , Eqs. (15), (21) and (22) determine the expressions for the rates of variation.

$$\dot{\Omega} = -\frac{3nJ_2R_T^2 \cos(i)}{2a^2(1-e^2)^2}. \quad (21)$$

$$\dot{M} = n - \frac{3J_2nR_T^2(3\cos(2i) + 1)}{8a^2(1-e^2)^{3/2}}. \quad (22)$$

Through the expressions of variations and taking an initial estimate for the value of the semi-major axis based on Eq. (19) and values for the inclination  $i$  and eccentricity  $e$  a more refined value, Eq. (23), considering the perturbation  $J_2$ , can be found for the semi-major axis of the orbit that will maintain the property of repeated trajectories.

$$a = \mu^{1/3} \left[ \frac{N_p}{N_d} (\theta - \dot{\Omega}) - (\dot{\omega} + \dot{M}_h) \right]^{-2/3}. \quad (23)$$

Having determined the regions of interest on surface of Titan and defined the necessary orbital requirements, in order to analyze the dynamics in the regions around Titan, an investigation into the influence of the perturbative forces coming from Saturn, the natural satellites closest to Titan and due to the non-sphericity of Titan will be realized.

#### Dynamical environment

As a first step in analyzing perturbation effects from Saturn and nearby natural satellites (Dione, Rhea, Hyperion, and Iapetus), it is calculated their gravitational accelerations on a satellite around Titan. Additionally, it is computed the accelerations caused by Titan's gravitational force, including its main harmonic coefficients  $J_2$ ,  $J_3$ ,  $J_4$ , and  $C_{22}$ .

Analyzing the magnitude of these forces is crucial, as it helps identify the degree of influence these disturbances have at different altitudes, thereby determining which should be considered in the proposed models to derive the elements of the nominal orbits such as the eccentricity  $e$ , argument of the pericenter  $\omega$ , and semi-major axis  $a$ , define the constellation. The results obtained are shown in Fig. 2. The analysis was conducted based on the altitude of a probe's orbit,

measured from the center of the satellite, within a range 1.0 to 30.0  $R_{Titan}$ , where 1  $R_{Titan}$  corresponds to the surface of the natural satellite. Additionally, the vertical black dotted line marks the altitude of an equatorial and synchronous orbit around Titan. The blue and red dashed lines indicate the boundary regions where atmospheric drag affects the natural satellite, representing altitudes with lower (red) and higher (blue) atmospheric density (Hörst, 2017).

The results show that among Titan's harmonic disturbances,  $J_2$  and  $C_{22}$  are the most significant. These terms dominate over the perturbations caused by other natural satellites up to approximately 10 Titan radii in altitude. At higher altitudes, the influence of the natural satellites gradually increases until it dominates that of the harmonic terms.

At altitudes above 20 Titan radii, the third-body effect due to Saturn becomes stronger than Titan's own gravitational attraction. Consequently, in the case of synchronous orbits around Titan, perturbations from Saturn and other natural satellites play a dominant role, making their inclusion in the dynamical model essential for higher precision.

Besides, depending on the perturbing body's inclination or eccentricity, these effects can be magnified, affecting both short-term and long-term variations and contributing to the potential loss of the desired formation.

It can be seen in Fig. 3 that, for the altitude interval between 1.5  $R_{Titan}$  and 5.0  $R_{Titan}$ , corresponding to an altitude from 3,862 km to 12,875 km, the gravitational

force of Titan has the greatest magnitude, followed by the perturbative effects from Saturn.

Among the harmonic coefficients of Titan, the results indicate that the zonal coefficient  $J_2$  has the greatest influence on the dynamics, followed by the sectorial coefficient  $C_{22}$ . That means that the non-uniformity of Titan's poles is responsible for greater disturbances than the irregular shape of its equator. However, the more equatorial the orbits are, the more strongly they are influenced by the sectorial perturbation  $C_{22}$ .

This highlights the fact that, although the polar orbits are affected by the perturbations, the more equatorial orbits will tend to be more disturbed by the harmonic coefficients.

Considering the altitude range up to 3.5  $R_{Titan}$  it can be seen that the harmonics  $J_3$  and  $J_4$  have a greater influence than the other natural satellites. From this altitude onwards, the contributions from the other natural satellites become dominant, with Rhea contributing the most, followed by Dione.

The acceleration promoted by each of the natural satellites is in the order range between  $10^{-13}$  and  $10^{-11}$   $\text{km/s}^2$ . The other harmonic coefficients  $J_3$  and  $J_4$  make the smallest contributions in terms of acceleration.

After analyzing the perturbations affecting a spacecraft orbiting Titan at different altitudes, the next step is to design a satellite constellation, taking into account all the previous analysis.

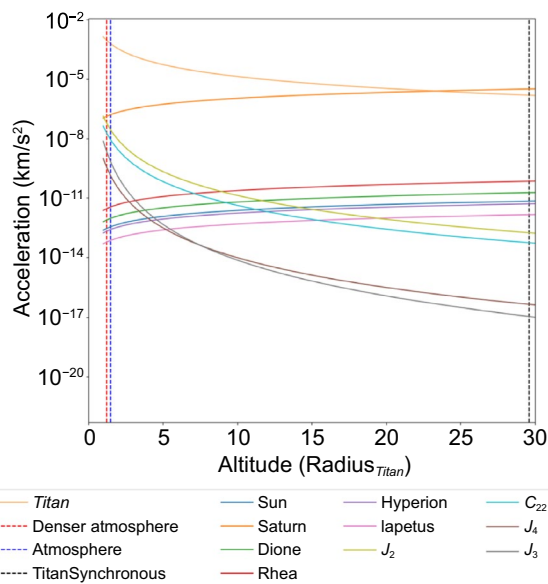


**Fig. 2** Acceleration of perturbation forces due to the Sun, Saturn (as nearby natural satellite), and Titan's harmonic coefficients ( $J_2$ ,  $J_3$ ,  $J_4$ , and  $C_{22}$ ), considering satellite altitudes up to 30 Titan radii

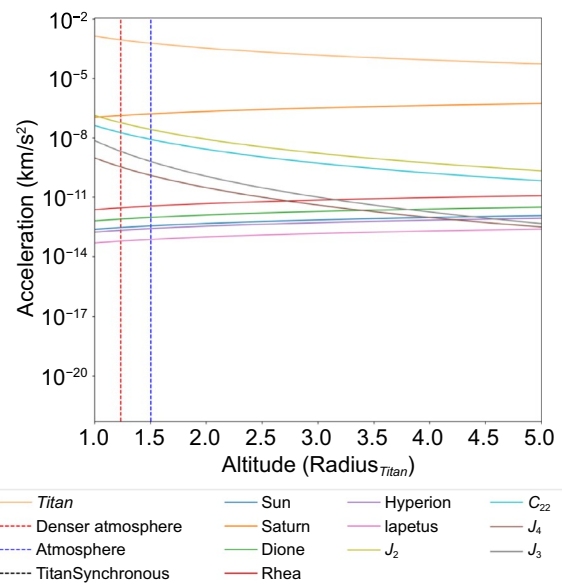


**Fig. 3** Acceleration of perturbation forces due to the Sun, Saturn (as nearby natural satellite), and Titan's harmonic coefficients ( $J_2$ ,  $J_3$ ,  $J_4$ , and  $C_{22}$ ), considering satellite altitudes to 5.0 Titan radii

**Table 2** Repetition parameters of compatible orbits

$N_p$	$N_d$	$Q$	a (km)	$N_p$	$N_d$	$Q$	a (km)
8	1	8.0	18891.50	39	4	9.8	16557.32
9	1	9.0	17464.84	41	4	10.2	16014.39
10	1	10.0	16280.20	42	5	8.4	18286.90
11	1	11.0	15277.93	43	4	10.8	15513.89
12	1	12.0	14416.91	43	5	8.6	18002.28
13	1	13.0	13667.76	45	4	11.2	15050.75
17	2	8.5	18143.19	47	4	11.8	14620.69
19	2	9.5	16846.54	47	5	9.4	16965.80
21	2	10.5	15759.18	48	5	9.6	16729.34
23	2	11.5	14831.82	49	4	12.2	14220.09
23	3	7.7	19435.18	51	4	12.8	13845.85
25	2	12.5	14029.85	52	5	10.4	15860.03
25	3	8.3	18384.30	53	5	10.6	15659.90
26	3	8.7	17909.84	55	7	7.9	19119.80
28	3	9.3	17046.50	57	5	11.4	14918.43
29	3	9.7	16652.34	57	7	8.1	18669.89
31	3	10.3	15928.18	58	5	11.6	14746.46
31	4	7.8	19295.61	62	5	12.4	14105.18
32	3	10.7	15594.59	62	7	8.9	17652.14
33	4	8.2	18507.90	63	5	12.6	13955.52
34	3	11.3	14976.88	64	7	9.1	17282.44
35	3	11.7	14690.23	69	7	9.9	16437.12
35	4	8.8	17795.94	71	7	10.1	16126.97
37	3	12.3	14155.96	76	7	10.9	15411.66
37	4	9.2	17148.73	78	7	11.1	15147.07
37	5	7.4	19899.33	83	7	11.9	14532.48
38	3	12.7	13906.51	85	7	12.1	14303.61
38	5	7.6	19548.67	90	7	12.9	13768.82

**Table 3** Repetition parameters to four specific cases

(a)	$N_p$	$N_d$	$Q$	a (km)
	37	5	7.4	19899.33
	38	5	7.6	19548.67
(b)	$N_p$	$N_d$	$Q$	a (km)
	13	1	13.0	13667.76
	90	7	12.9	13768.82

(a): Two cases with the lowest values of the  $Q$  parameter and (b): Two smallest values for the initial semi-major axis

### Satellite constellation design and evaluation

In this section, the constellations will be designed taking into account the orbital characteristics of trajectory repetition and frozen orbits discussed in section “[Design requirements](#)”, considering 2D-NFC methodology. Two constellations will be presented considering the different targets proposed in section “[Mission requirements](#)” one aims to cover the lakes and seas of Titan, Constellation

Titan I, and the other one focuses on the equatorial region of Titan, Constellation Titan II. Once the constellations were designed, the main disturbances presented in section “[Satellite constellation design](#)” were considered in order to analyze the long-term behavior of the constellations.

**Table 4** Admissible parameters for constellation design considering parameters  $N_p = 37$  and  $N_d = 5$ .

$N_{fso}$	$N_{rso}$	$k$	Necklace
5	1	3	{1}
5	2	3	{1, 2}
5	2	3	{1, 3}
5	3	3	{1, 2, 3}
5	3	3	{1, 2, 4}
5	4	3	{1, 2, 3, 4}
5	5	0	{1, 2, 3, 4, 5}

In all cases the phasing parameter is  $N_c = 1$

**Table 5** Admissible parameters for constellation design considering parameters  $N_p = 38$  and  $N_d = 5$ .

$N_{fso}$	$N_{rso}$	Necklace
5	1	{1}
5	2	{1, 2}
5	2	{1, 3}
5	3	{1, 2, 3}
5	3	{1, 2, 4}
5	4	{1, 2, 3, 4}
5	5	{1, 2, 3, 4, 5}

In all cases the value of the phasing and symmetry parameter is  $N_c = k = 0$

**Table 6** Admissible parameters for the constellation design considering the parameters  $N_p = 90$  and  $N_d = 7$ .

$N_{fso}$	$N_{rso}$	Necklace
7	1	{1}
7	2	{1, 2}
7	2	{1, 3}
7	2	{1, 4}
7	3	{1, 2, 3}
7	3	{1, 2, 4}
7	3	{1, 3, 4}
7	3	{1, 2, 5}
7	3	{1, 3, 5}
7	4	{1, 2, 3, 4}
7	4	{1, 2, 3, 5}
7	4	{1, 2, 4, 5}
7	4	{1, 3, 4, 5}
7	4	{1, 2, 4, 6}
7	5	{1, 2, 3, 4, 5}
7	5	{1, 2, 3, 4, 6}
7	5	{1, 2, 3, 5, 6}
7	6	{1, 2, 3, 4, 5, 6}
7	7	{1, 2, 3, 4, 5, 6, 7}

In all cases the value of the phasing and symmetry parameter is  $N_c = k = 0$

## Repeated ground-tracks and Necklace Flower

### Constellations methodology

It has been shown that in the 2D-NFC model, the orbits that compose the constellation share the same values for the orbital elements semi-major axis ( $a$ ), inclination ( $I$ ), eccentricity ( $e$ ) and argument of the pericenter ( $\omega$ ) (Casanova et al., 2011, 2014). The first step in this investigation was to determine the possible values for the semi-major axis of the orbits, taking into account the property of trajectory repetition by the artificial satellites involved. In this case, the disturbance due to the zonal harmonic  $J_2$  was considered.

Based on Eq. (19) the possible initial values for the semi-major axis, in terms of the values of  $N_p$  and  $N_d$ , were obtained taking as physical constraints the acceptable initial altitude range and the number of orbits per sidereal day ( $Q$ ), defined by  $Q = N_p/N_d$ , for each of the satellites. In terms of the altitude range, taking as references previous works such as Waite et al. (2013), Ferreira et al. (2022), assuming a safety altitude relative to the effects of atmospheric drag with a value of  $Alt_{min} = 1,400$  km and the maximum limit as  $Alt_{max} = 20,000$  km, since, due to the strong disturbance promoted by Saturn, the intention was to allocate the constellations as close as possible to Titan. This range, in terms of Titan radii, corresponds to altitudes in the range of 0.54 to 7.77 Titan radii. As for the number of orbits per day, we considered a maximum value of  $Q = 13$ , since the repetition frequency depends on the radius of the celestial body.

Based on Eq. (19) and the constraints considered, the initial values for the semi-major axis in terms of the parameters  $N_p$  and  $N_d$  that meet the proposed requirements were obtained and recorded in Table 2. Among these values, Table 3 shows in item (a) the two conditions with the lowest values for the  $Q$  parameter. Thus, these orbits are those whose space vehicles have the lowest number of revolutions per day. This promotes a longer interval between revisits and possible data collection. Table 3 shows in item (b) the two configurations with the lowest values obtained for the semi-major axis, which corresponds to the lower orbits. Considering that for orbits around natural satellites the third body disturbances are more intense, these orbits, closer to the satellites, tend to be more stable because they are less affected by the disturbances coming from the third body.

Based on the configurations established in Table 3, the values of the parameters related to the constellation design were determined. These values generate configurations for the initial distribution of the constellation, allowing all involved satellites to share the trajectory and maintain the property of orbital repetition.

For this study, we fixed the number orbital planes  $N_0 = 2$  and a range  $2 \leq N_{fso} \leq 10$  for the number of



**Table 7** Admissible parameters for constellation design considering three real satellites in each orbital plane

$N_p$	$N_d$	$N_{fso}$	$N_{rso}$	$N_c$	$k$	Necklace
37	5	5	3	1	3	{1, 2, 3}
37	5	5	3	1	3	{1, 2, 4}
38	5	5	3	0	0	{1, 2, 3}
38	5	5	3	0	0	{1, 2, 4}
90	7	7	3	0	0	{1, 2, 3}
90	7	7	3	0	0	{1, 2, 4}
90	7	7	3	0	0	{1, 3, 4}
90	7	7	3	0	0	{1, 2, 5}
90	7	7	3	0	0	{1, 3, 5}

fictitious satellites were assumed based on the altitude range established in this paper, and results presented for other design methodologies that show a range of up to 20 satellites for the same altitude range (Lang & Adams, 1998). As  $N_{rso} \leq N_{fso}$ , a range of  $1 \leq N_{rso} \leq N_{fso}$  for the number of real satellites in each orbital plane of the constellation was considered. Since it is known that the necessary condition presented in Eq. (9) guarantees that the satellites involved in the constellation have the same trajectory in the relative system, the conditions obtained that satisfy the necessary conditions, combined with the possible necklaces, are presented in Tables 4, 5 and 6.

Considering the range assumed for the parameters related to the design of the constellations, no admissible parameter sets were found for the conditions  $N_p = 13$  and  $N_d = 1$ . Based on the theory of Necklace Flower Constellations, this result is due to the condition of divisibility and maximum common divisor that must be valid in conjunction with Eq. (9). As the coefficient  $N_d = 1$ , within the proposed range the preliminary conditions were not satisfied, so there are no admissible parameters that form the designs (Arnas et al., 2021). The divisibility condition can also be observed in the results obtained in Tables 4, 5 and 6 since within a range of [1, 20], the only possible configurations for the number of fictitious positions for the designs are equal to the parameter  $N_d$  because they are the only values in the range that guarantee the required divisibility conditions.

In this work we consider three satellites in each orbital plane, giving a total of 6 satellites in the entire constellation. This selection is based on previous work, Gaur and Prasad (2020), related to Earth and Mars that indicates a minimum number of 6 satellites for missions related to global coverage. Thus, the sets of admissible parameters assumed were gathered in Table 7.

In the next section, the drawings, phase spaces, and propagation of some designs from Table 7 will be presented. So far, the 2D Necklace Flower Constellation methodology has been described, along with the

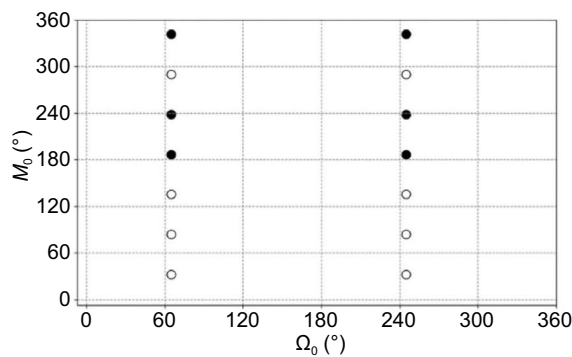
admissible semi-major axis values that ensure a repeating ground-track trajectory and the eccentricity and argument of perigee values that provide frozen orbits. The selected points of interest for the initial satellite position in the formation will be introduced, including the right ascension of the ascending node and the mean anomaly, while also establishing the inclination, eccentricity, and argument of pericenter values that promote frozen orbits. Finally, the evolution of the constellation's orbits will be analyzed, followed by a preliminary study of the effects of other perturbations. Two different satellite constellations will be presented: the first aims to cover Titan's lakes and seas in near-polar regions, while the second focuses on the equatorial regions where dunes and Hummocky are found.

### Constellation Titan I

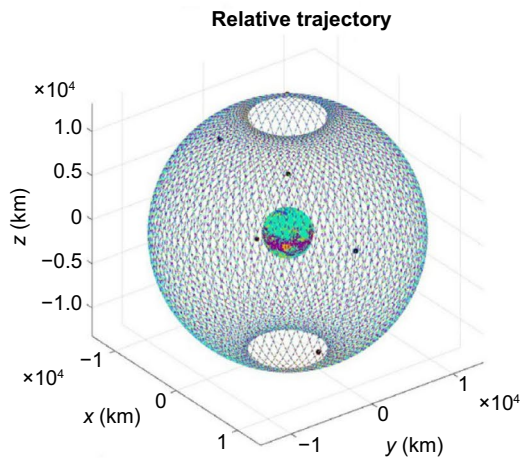
As the main objective of Constellation Titan I is to cover the regions of lakes and seas of Titan, the regions in yellow on the map in Fig. 1, the condition  $N_p = 90$  and  $N_d = 7$ , Table 7, and the design with the necklace  $\mathcal{G} = \{1, 2, 4\}$  was considered. Given that the model needs a reference satellite that will be the first satellite of the formation in the first inertial orbit, with a position in phase space  $\Omega_{11}$  and  $M_{11}$ , we consider the Ontario Lacus region, point (09), as this location.

As the constellation has a repeating trajectory, this point will be visited by all the spacecraft that formed the constellation based on the revisit rate assumed by the parameters  $N_p$  and  $N_d$ . Based on the latitude and longitude coordinates of Ontario Lacus Lake, the values for the longitude of the node  $\Omega_{11}$  and for the mean anomaly  $M_{11}$  were obtained. Considering the latitude of the site of interest, 72 degrees, we assumed an inclination of 73.3572 degrees for the two nominal orbits. This inclination requires  $e = 4.946302974736958 \times 10^{-4}$  to guarantee the properties of frozen orbits.

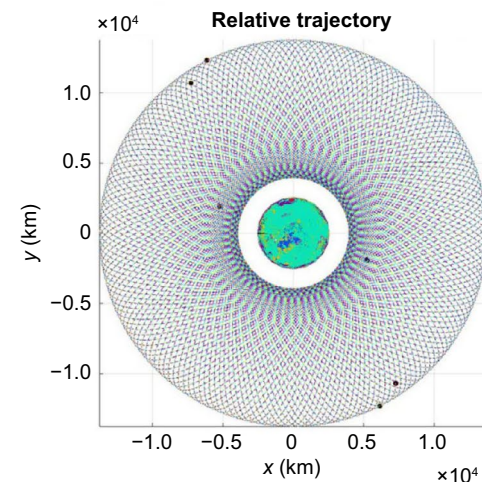
Figure 4 shows the  $(\Omega, M)$ -space generated by the 2D-NFC methodology, and a 3D modeling of the



a



b



c

**Fig. 4** The  $(\Omega, M)$ -space (a), 3D Orbit Scheme in the Relative System (b)–(c):  $N_o = 2$ ,  $N_c = 0$ ,  $Sym = 0$ ,  $N_{iso} = 7$ ,  $N_{so} = 3$ ,  $N_p = 90$ ,  $N_d = 7$ ,  $a = 5.3482 R_{Titan}$ ,  $e = 4.946302 \times 10^{-4}$ ,  $i = 73.3572^\circ$ ,  $\Omega_{11} = 63.92^\circ$ ,  $M_{11} = 186.96^\circ$  and necklace  $\mathcal{G} = \{1, 2, 4\}$

constellation. The black dots correspond to the positions of the satellites in the orbit which are separated in terms of their longitudes of the ascending node of 180 degrees. The white dots combined with the black dots correspond to the admissible positions for the vehicles based on the 2D-NFC methodology. In Fig. 4b,c the observed orbits were generated considering the relative system, and it is possible to see that the satellites involved shared the trajectory.

The propagations in the inertial and relative systems of the trajectories of the space vehicles on the surface of Titan can be seen in Figs. 5 and 6, where the  $J_2$  and  $J_3$  effects are considered.

On the maps, the black diamonds correspond to the initial positions of the satellites that compose the constellation. The ground-track of Fig. 5 shows that for the simulation time considered, the regions of interest, especially Ontario Lacus, (09), and Kraken Mare, (02), are covered by the relative trajectories of the vehicles. The other regions at lower latitudes end up being covered at some point due to the inclination imposed on the constellation.

### Constellation Titan II

The aim of Constellation Titan II is to fly over the regions closest to Titan's equator. To do this, the conditions  $N_p = 38$  and  $N_d = 5$ , and  $N_p = 90$  and  $N_d = 7$  were considered, so it is possible to observe the perturbation effects due to the different altitudes since the more equatorial orbits suffer more from the effects of the  $J_2$  and  $C_{22}$  harmonic perturbations.

Among the admissible designs in Table 7, the necklace  $\mathcal{G} = \{1, 2, 4\}$  was maintained. For this approach, Huygens Landing, (01), was taken as the position of the constellation's reference satellite. Considering the model to determine the frozen conditions, the constellations implemented assumed an inclination of 11.24 degrees and 11.74 degrees, respectively, and eccentricities of  $e = 11243004449633647 \times 10^{-4}$  and  $e = 7.9 \times 10^{-5}$ .

After performing the transformation between latitude–longitude to Right Ascension of the Ascending Node - Mean Anomaly, the values obtained for the Right Ascension of the Ascending Node and the Mean Anomaly for the orbits of the initial satellites, in the two considered cases were  $\Omega_{11} = 57.49^\circ$ ,  $M_{11} = 199.81^\circ$  and  $\Omega_{11} = 51.49^\circ$ ,  $M_{11} = 205.70^\circ$ , respectively.

Figures 7 and 8 show the  $(\Omega, M)$ -space generated by the 2D-NFC methodology, and a 3D modeling of the constellation, and the Figs. 9 and 10 and Figs. 11 and 12 present the ground-tracks in the inertial and relative systems of the trajectories of the space vehicles on Titan's surface for



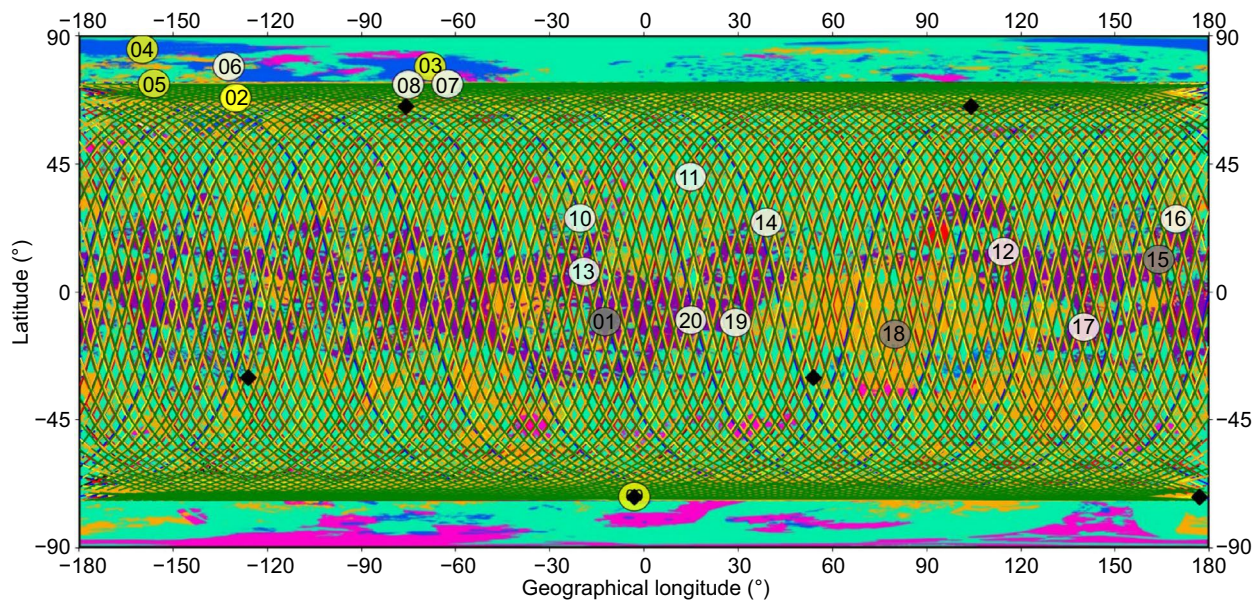


**Fig. 5** Orbital evolution of satellites, in the relative system, to Constellation Titan I with orbital parameters:  $N_o = 2, N_c = 0, Sym = 0, N_{fso} = 7, N_{rso} = 3, N_p = 90, N_d = 7, a = 5.3482 R_{Titan}, e = 4.946302 \times 10^{-4}, i = 73.3572^\circ, \Omega_{11} = 63.92^\circ, M_{11} = 186.96^\circ$  and necklace  $\mathcal{G} = \{1, 2, 4\}$

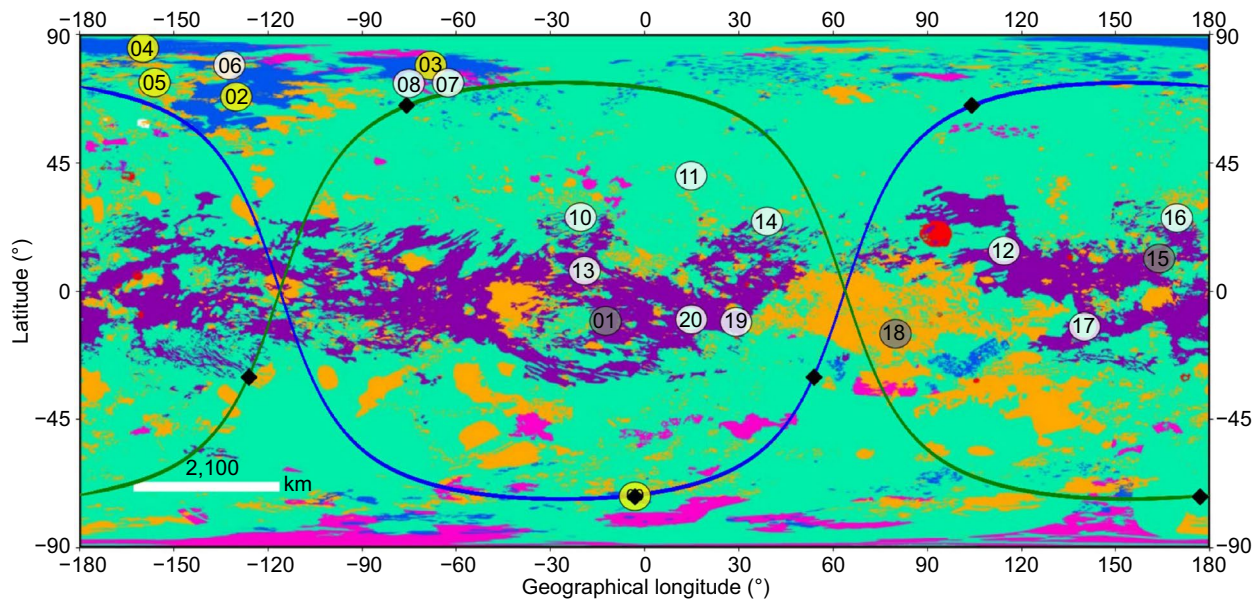


**Fig. 6** Orbital evolution of satellites, in the inertial system, to Constellation Titan I with orbital parameters:  $N_o = 2, N_c = 0, Sym = 0, N_{fso} = 7, N_{rso} = 3, N_p = 90, N_d = 7, a = 5.3482 R_{Titan}, e = 4.946302 \times 10^{-4}, i = 73.3572^\circ, \Omega_{11} = 63.92^\circ, M_{11} = 186.96^\circ$  and necklace  $\mathcal{G} = \{1, 2, 4\}$

each condition of repeating Ground-Tracks, where the  $J_2$  and  $J_3$  effects are considered.

#### Long-term analysis

The initial conditions of the satellite constellations presented in the previous section were numerically integrated to evaluate their orbital evolution. Two dynamical

environments were considered for this analysis. The first scenario includes only the perturbations due to the  $J_2$  and  $J_3$ , which were incorporated into the orbit design (frozen and repetition ground-track). The second scenario adds the perturbative effects from the coefficient  $C_{22}$  and third-body perturbation due to Saturn.

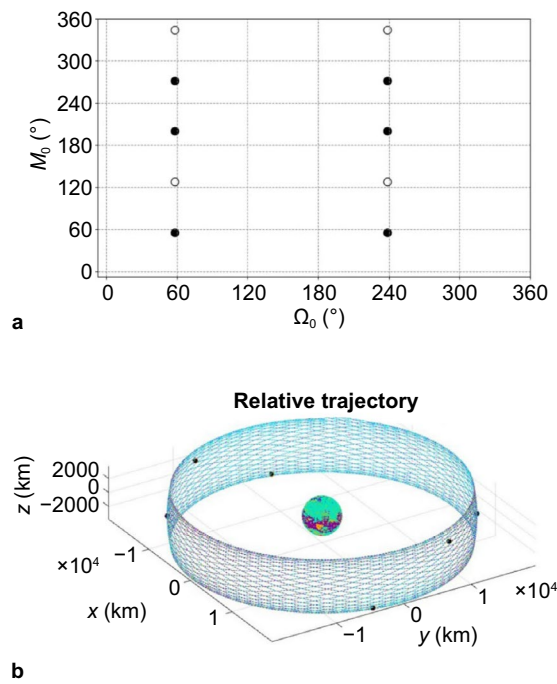


**Fig. 7** The  $(\Omega, M)$ -space (a) and 3D Orbit Scheme in the Relative System (b). Orbital parameters  $N_o = 2, N_c = 0, Sym = 0, N_{fso} = 7, N_{rso} = 3, N_p = 38, N_d = 5, a = 7.5952 R_{Titan}, e = 7.5 \times 10^{-5}, i = 11.24^\circ, \Omega_{11} = 57.49^\circ, M_{11} = 199.81^\circ$  and necklace  $\mathcal{G} = \{1, 2, 4\}$

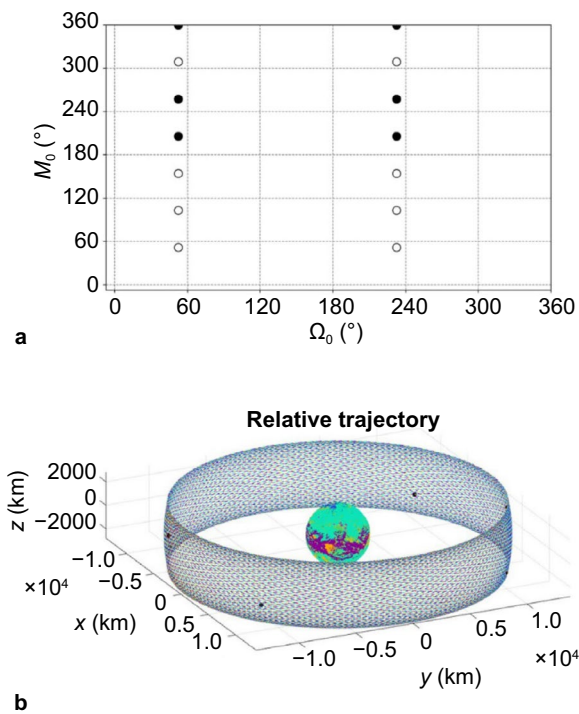


**Fig. 8** The  $(\Omega, M)$ -space (a), 3D Orbit Scheme in the Relative System (b) and orbital evolution of satellites with orbital parameters (c):  $N_o = 2, N_c = 0, Sym = 0, N_{fso} = 7, N_{rso} = 3, N_p = 90, N_d = 7, a = 5.3495 R_{Titan}, e = 0.000112, i = 11.74^\circ, \Omega_{11} = 51.49^\circ, M_{11} = 205.70^\circ$  and necklace  $\mathcal{G} = \{1, 2, 4\}$

It was examined how these perturbations affect the dynamics of the satellites. For this purpose, the Constellation Titan I and Constellation Titan II designs were considered.

Figures 13 and 14 present the phase diagram of  $e \sin(\omega) \times e \cos(\omega)$ , and the evolution of the eccentricity. The red lines correspond to the simulations considering a scenario with the perturbation due to the  $J_2$  and  $J_3$  harmonic coefficients. The black lines correspond to the simulations considering in addition the perturbations from the disturbing coefficient  $C_{22}$  and the third-body perturbation due to Saturn. The simulations include the evolution of all six satellites present in the constellation, that is why there are six black lines in Fig. 13.

The simulations were conducted considering a criterion for spacecraft orbit loss at an altitude of 1300 km, a region where the effects of atmospheric drag become more significant. The blue dotted line in Figs. 13 and 14 corresponds to the eccentricity value over which the probe is lost because its altitude is equal to or less than 1,300 km. In this way, the time during which the satellites in the constellation remain outside the region affected by atmospheric drag, once the disturbances are considered in the system, was analyzed. This interval is crucial as it determines the period during which corrective maneuvers can be performed to return the vehicles to their designated positions within the constellation.

Figures 13b and 14b present the evolution of the eccentricity.

In particular, the vehicles of the most equatorial constellation, Constellation Titan II, remain outside the atmospheric drag region during the 5 years of integration. Even though the eccentricities of the orbits were affected by third-body perturbations and Titan's  $C_{22}$  coefficient, these vehicles were not affected by atmospheric drag. However, in the case of Constellation Titan I, the configuration is not preserved, since one of the satellites falls over the region of atmospheric drag action in a time interval of approximately 2.7 months. Note that corrective maneuvers can be performed at any time as long as there is no influence from atmospheric drag.

This behavior is to be expected, since the inclination of Constellation Titan I is almost polar. Thus, the effects due to the Kozai-Lidov mechanism are more pronounced. Lower orbits experience fewer of these disturbances. Previous work, Ferreira et al. (2022) reinforces these results by generating maps of surviving regions around Titan, taking Saturn's perturbations into account.

In terms of the properties of frozen orbits, the phase diagrams in Figs. 13a and 14a present that for the full simulation interval considered, the vehicles' orbits preserve the frozen conditions when simulated considering the effects due to the  $J_2$  and  $J_3$  harmonics.



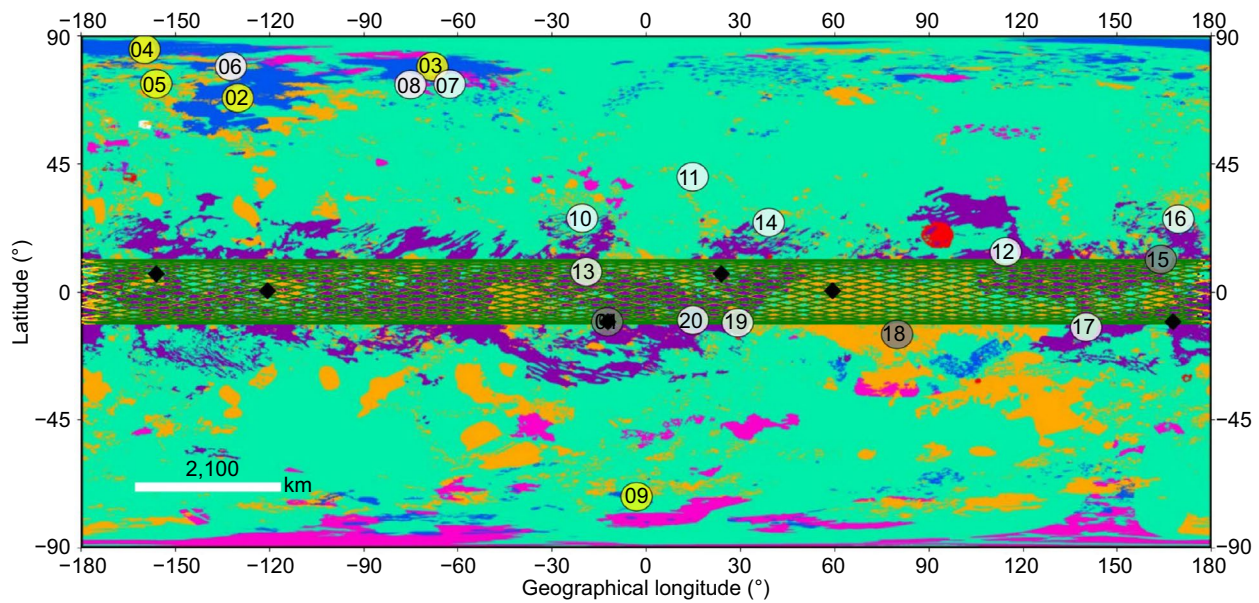


**Fig. 9** Orbital evolution of satellites, in the relative system, to Constellation Titan II with orbital parameters:  $N_o = 2, N_c = 1, Sym = 3, N_{fso} = 7, N_{rso} = 3, N_p = 38, N_d = 5, a = 7.5952 R_{Titan}, e = 7.5 \times 10^{-5}, i = 11.24^\circ, \Omega_{11} = 57.49^\circ, M_{11} = 199.81^\circ$  and necklace  $\mathcal{G} = \{1, 2, 4\}$

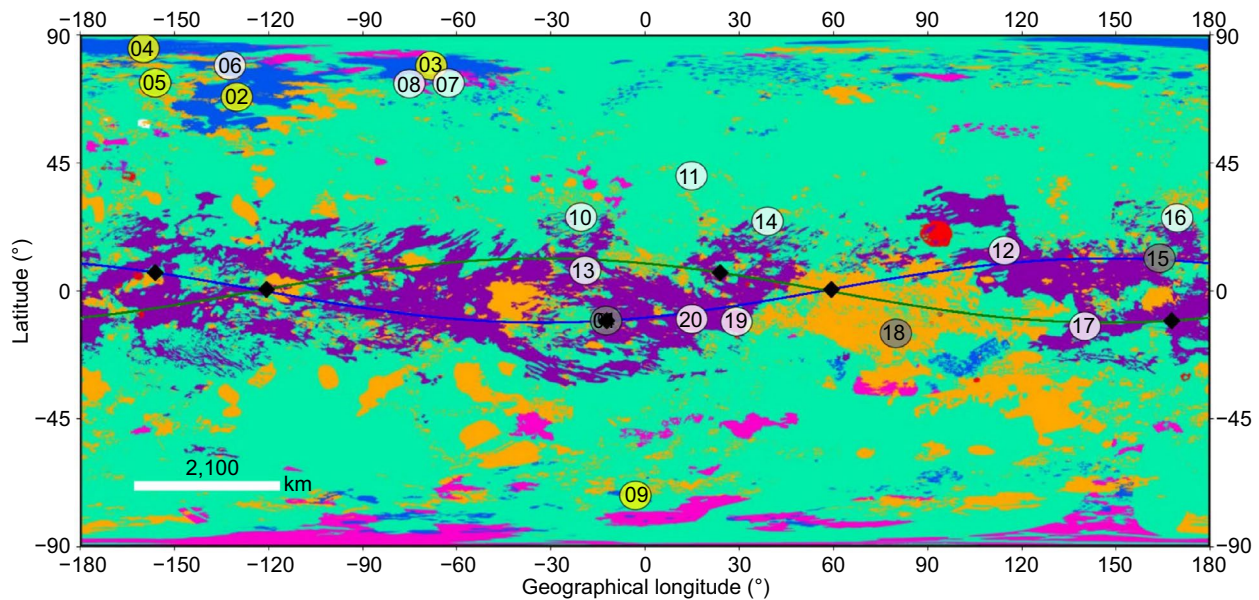


**Fig. 10** Orbital evolution of satellites, in the inertial system, to Constellation Titan II with orbital parameters:  $N_o = 2, N_c = 1, Sym = 3, N_{fso} = 7, N_{rso} = 3, N_p = 38, N_d = 5, a = 7.5952 R_{Titan}, e = 7.5 \times 10^{-5}, i = 11.24^\circ, \Omega_{11} = 57.49^\circ, M_{11} = 199.81^\circ$  and necklace  $\mathcal{G} = \{1, 2, 4\}$

## Conclusions

This investigation aims to contribute to research into exploring the natural satellite Titan. To this end, the study considered the 2D-Necklace Flower Constellation (2D-NFC) methodology for the design of the constellations because, using the concepts of modularity and symmetry, this methodology maximizes the possible orbital

configurations by combining techniques from Flower Constellation Theory with Necklaces Theory. In this sense, 2D-NFC was used to optimize the distribution and dynamics of the satellites. Based on previous work, some areas of interest were highlighted for overflight on Titan. Priority was given to two groups of regions, one focused on Titan's lakes and seas (Constellation Titan I) and the



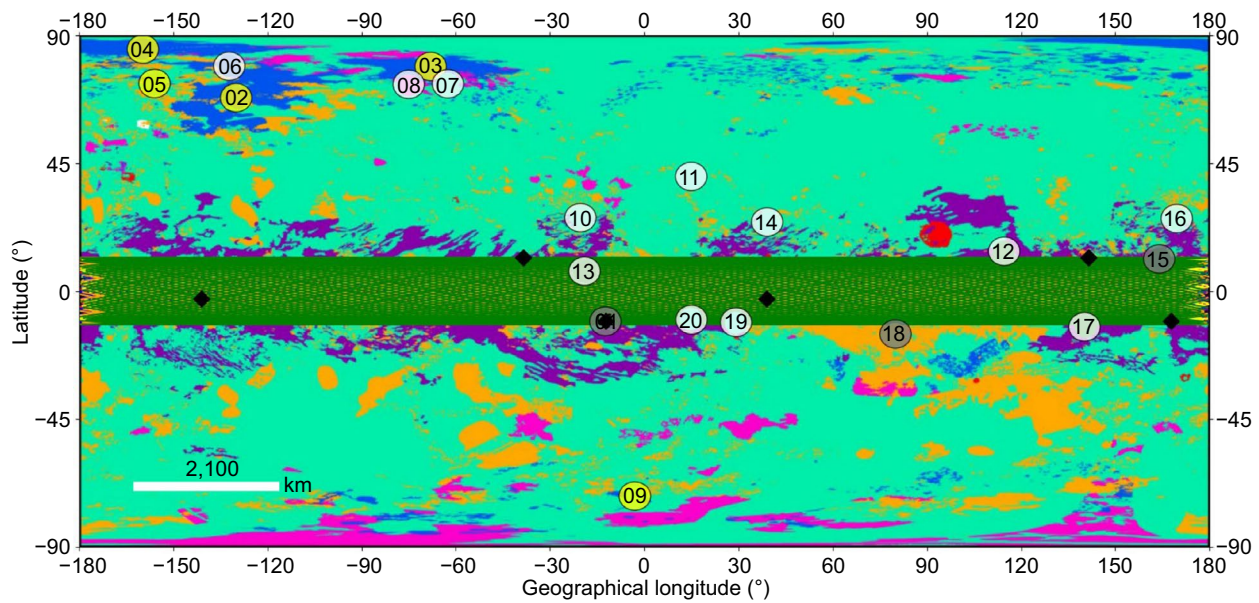


**Fig. 11** Orbital evolution of satellites, in the relative system, to Constellation Titan II with orbital parameters:  $N_o = 2, N_c = 0, Sym = 0, N_{fso} = 7, N_{rso} = 3, N_p = 90, N_d = 7, a = 5.3495 R_{Titan}, e = 0.000112, i = 11.74^\circ, \Omega_{11} = 51.49^\circ, M_{11} = 205.70^\circ$  and necklace  $\mathcal{G} = \{1, 2, 4\}$

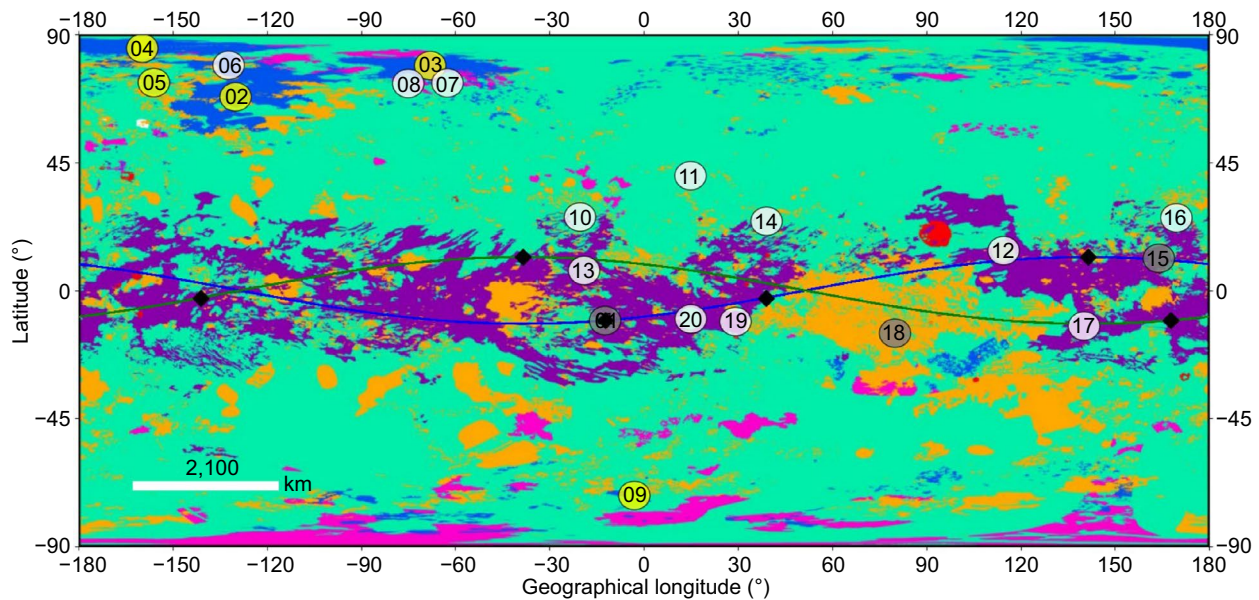


**Fig. 12** Orbital evolution of satellites, in the inertial system, to Constellation Titan II with orbital parameters:  $N_o = 2, N_c = 0, Sym = 0, N_{fso} = 7, N_{rso} = 3, N_p = 90, N_d = 7, a = 5.3495 R_{Titan}, e = 0.000112, i = 11.74^\circ, \Omega_{11} = 51.49^\circ, M_{11} = 205.70^\circ$  and necklace  $\mathcal{G} = \{1, 2, 4\}$

other on the more equatorial regions (Constellation Titan II). Three examples of constellations were presented, with the number of orbital planes in all cases being two ( $N_o = 2$ ). Considering that in 2D-NFC, the orbital elements  $a, e, i$  and  $\omega$  are common to all the orbits that make up the constellation, the initial semi-major axes that promote the ground-track repetition property were

assumed. An altitude range of 1,400km to 20,000km was considered as well as a number of orbital periods per day  $Q = 13$ . In this sense, the two conditions  $N_p$  and  $N_d$  that promoted orbits with the lowest semi-major axis values within the range considered were highlighted. As well as the two conditions with the lowest number of orbital periods per day. The eccentricity, inclination, and

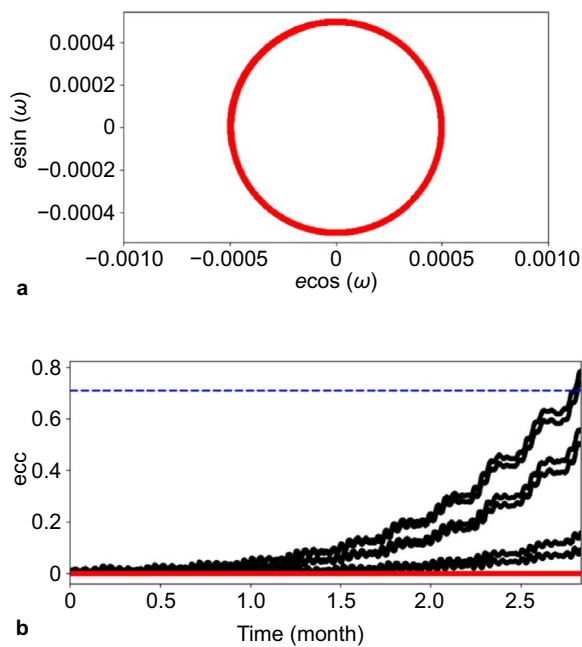


**Fig. 13** Phase diagram of  $e \sin(\omega) \times e \cos(\omega)$ , (a), and orbital evolution of the eccentricity, (b). Constellation Titan I -  $N_p = 90$  and  $N_d = 7$ . In red the dynamics with  $J_2$  and  $J_3$  and in black  $J_2 + J_3 + C_{22} + Saturn$

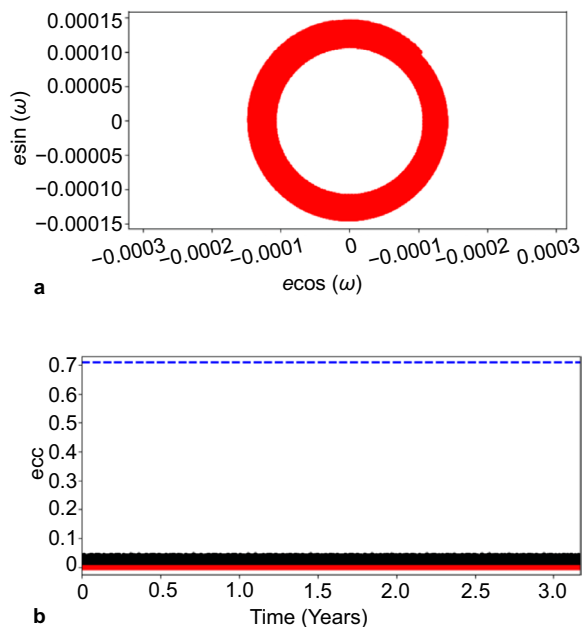


**Fig. 14** Phase diagram of  $e \sin(\omega) \times e \cos(\omega)$ , (a), and orbital evolution of the eccentricity, (b). Constellation Titan II -  $N_p = 90$  and  $N_d = 7$ . In red the dynamics with  $J_2$  and  $J_3$  and in black  $J_2 + J_3 + C_{22} + Saturn$

argument of the pericenter for obtaining frozen orbits, assuming a model containing Titan's  $J_2$  and  $J_3$  zonal harmonics, were also considered. The other elements were generated considering the 2D-Necklace Flower Constellation model. A total number of 6 satellites per constellation was assumed, and the parameters of the design were established.

Finally, an investigation into the evolution of the eccentricity of the satellites' orbit was done considering two scenarios: the first scenario, incorporated into the orbit design (frozen and repetition ground-track), includes only the perturbations due to the  $J_2$  and  $J_3$  and a second scenario, whereas the perturbative effects from the coefficient  $C_{22}$  and third-body perturbation due to Saturn was assumed. Considering the research in this investigation, future studies related to planning corrective orbital maneuvers that aim to keep the satellites within the desired formation criteria and relocate these spacecraft to their initial positions are motivated. Investigations of coverage times and distributions considering different approaches can also be carried out.

#### Acknowledgements

Not applicable.

#### Author contributions

L.S.F., D.C., and E.T. proposed the concept of this paper. D.C. and E.T. guidance of the manuscript. D.C., E.T., and A.F.B.A.P. help with the writing. All authors have read and approved the final manuscript.

#### Funding

The work of L.Ferreira and A.F.B.A Prado has been supported by Program CAPES-PDSE, process number 88881.982568/2024-01, and São Paulo Research Foundation (FAPESP) [grant number 2022/11783-5]. The work of D. Casanova and E. Tresaco have been supported by Grant PID2024-156002NB-I00 funded by MICIU/AEI/10.13039/501100011033/FEDER, UE, and by the Aragón Government and European Social Fund (E24\_23R).

#### Data availability

The datasets generated during and/or analysed during the current study are available from the corresponding author on reasonable request.

#### Declarations

#### Competing interests

All authors declare that they have no competing interests.

Received: 25 March 2025 Revised: 4 September 2025 Accepted: 18

September 2025

Published online: 30 October 2025

#### References

- Abad, A., Elife, A., & Tresaco, E. (2009). Analytical model to find frozen orbits for a lunar orbiter. *Journal of Guidance, Control, and Dynamics*, 32(3), 888–898.
- An, X., Meng, X., & Jiang, W. (2020). Multi-constellation GNSS precise point positioning with multi-frequency raw observations and dual-frequency observations of ionospheric-free linear combination. *Satellite Navigation*, 1(1), 1–13.

- Arnas, D., Casanova, D., & Tresaco, E. (2017). Time distributions in satellite constellation design. *Celestial Mechanics and Dynamical Astronomy*, 128(2), 197–219.
- Arnas, D., Casanova, D., Tresaco, E., & Mortari, D. (2017). 3-dimensional necklace flower constellations. *Celestial Mechanics and Dynamical Astronomy*, 129, 433–448.
- Arnas, D., Casanova, D., & Tresaco, E. (2018). 2D necklace flower constellations. *Acta Astronautica*, 142, 18–28.
- Arnas, D., Casanova, D., & Tresaco, E. (2021). 2D necklace flower constellations applied to earth observation missions. *Acta Astronautica*, 178, 203–215.
- Avendaño, M. E., Davis, J. J., & Mortari, D. (2013). The 2-D lattice theory of flower constellations. *Celestial Mechanics and Dynamical Astronomy*, 116, 325–337.
- Barnes, J. W., Brown, R. H., Soderblom, L., Buratti, B. J., Sotin, C., Rodriguez, S., Le Mouéllic, S., Baines, K. H., Clark, R., & Nicholson, P. (2007). Global-scale surface spectral variations on Titan seen from Cassini/VIMS. *Icarus*, 186(1), 242–258.
- Barnes, J. W., MacKenzie, S. M., Young, E. F., Soderblom, J. M., Hayes, A. G., Sotin, C., Brown, R. H., & Soderblom, L. A. (2020). Diffraction-limited Titan surface imaging from orbit using near-infrared atmospheric windows. *The Planetary Science Journal*, 1(1), 1–24.
- Casanova, D., Avendano, M., & Mortari, D. (2011). Necklace theory on flower constellations. *Advances in the Astronautical Sciences*, 140, 1791–1803.
- Casanova, D., Avendano, M. E., & Mortari, D. (2014). Design of flower constellations using necklaces. *IEEE Transactions on Aerospace and Electronic Systems*, 50(2), 1347–1358.
- Cinelli, M., Lei, H., Ortore, E., & Circi, C. (2022). Probe lifetime around natural satellites with obliquity. *Astrodynamics*, 6(4), 429–439.
- Circi, C., Ortore, E., & Bunkheila, F. (2014). Satellite constellations in sliding ground track orbits. *Aerospace Science and Technology*, 39, 395–402.
- Cornara, S., Beech, T. W., Belló-Mora, M., & Janin, G. (2001). Satellite constellation mission analysis and design. *Acta Astronautica*, 48(5–12), 681–691.
- De Almeida Prado, A. F. B. (2003). Third-body perturbation in orbits around natural satellites. *Journal of Guidance, Control, and Dynamics*, 26(1), 33–40.
- Delsate, N., Robutel, P., Lemaître, A., & Carletti, T. (2010). Frozen orbits at high eccentricity and inclination: Application to mercury orbiter. *Celestial Mechanics and Dynamical Astronomy*, 108, 275–300.
- Elpe, A., & Lara, M. (2003). Frozen orbits about the moon. *Journal of Guidance, Control, and Dynamics*, 26(2), 238–243.
- Ferreira, L. S., Sfair, R., & Prado, A. F. B. A. (2022). Lifetime and dynamics of natural orbits around Titan. *Symmetry*, 14(6), 1–25.
- Formiga, J. K. S., & Moraes, R. V. (2011). 15: 1 resonance effects on the orbital motion of artificial satellites. *Journal of Aerospace Technology and Management*, 3(3), 251–258.
- Gaur, D., & Prasad, M. S. (2020). Analysis of communication satellite array for optimal global coverage on mars. In *2020 8th International Conference on Reliability* (pp. 1064–1067). Infocom Technologies and Optimization (Trends and Future Directions)(ICRITO): IEEE.
- Gopalchetty, B., & Coates, A. J. (2025). TARA: Concept study for an ESA voyage titan exploration mission. *Experimental Astronomy*, 59(1), 1–25.
- Guo, F., Yang, Y., Ma, F., Zhu, Y., Liu, H., & Zhang, X. (2023). Instantaneous velocity determination and positioning using Doppler shift from a LEO constellation. *Satellite Navigation*, 4(1), 1–25.
- Hein, G. W. (2020). Status, perspectives and trends of satellite navigation. *Satellite Navigation*, 1(1), 1–25.
- Hörst, S. M. (2017). Titan's atmosphere and climate. *Journal of Geophysical Research: Planets*, 122(3), 432–482.
- Lang, T. J., & Adams, W. S. (1998). A comparison of satellite constellations for continuous global coverage. In *Mission design & implementation of satellite constellations: proceedings of an international workshop, held in Toulouse, France* (pp. 51–62). Springer.
- Lara, M., Deprit, A., & Elpe, A. (1995). Numerical continuation of families of frozen orbits in the zonal problem of artificial satellite theory. *Celestial Mechanics and Dynamical Astronomy*, 62, 167–181.
- Li, H., Luo, D., & Ding, H. (2023). Real-time service performances of BDS-3 and Galileo constellations with a linear satellite. *Satellite Navigation*, 4(1), 1–10.
- Li, R., Zheng, S., Wang, E., Chen, J., Feng, S., Wang, D., & Dai, L. (2020). Advances in BeiDou navigation satellite system (BDS) and satellite navigation augmentation technologies. *Satellite Navigation*, 1(1), 1–23.
- Liu, X., Baoyin, H., & Ma, X. (2011). Analytical investigations of quasi-circular frozen orbits in the Martian gravity field. *Celestial Mechanics and Dynamical Astronomy*, 109, 303–320.
- Lopes, R. M., Kirk, R. L., Mitchell, K. L., LeGall, A., Barnes, J. W., Hayes, A., Kargel, J., Wye, L., Radebaugh, J., Stofan, E. R., & Janssen, M. A. (2013). Cryovolcanism on Titan: New results from Cassini RADAR and VIMS. *Journal Of Geophysical Research-planets*, 118(3), 416–435.
- Lopes, R. M., Malaska, M. J., Schoenfeld, A., Solomonidou, A., Birch, S. P., Florence, M., Hayes, A. G., Williams, D. A., Radebaugh, J., Verlander, T., & Turtle, E. P. (2020). A global geomorphologic map of Saturn's moon titan. *Nature astronomy*, 4(3), 228–233.
- Lorenz, R. D., Leary, J. C., Lockwood, M. K., & Waite, J. H. (2008). Titan explorer: A NASA flagship mission concept. In *AIP Conference Proceedings, American Institute of Physics* (pp. 380–387).
- Lorenz, R. D., Turtle, E. P., Barnes, J. W., Trainer, M. G., Adams, D. S., Hibbard, K. E., Sheldon, C. Z., Zacny, K., Peplowski, P. N., Lawrence, D. J., & Ravine, M. A. (2018). Dragonfly: A rotorcraft lander concept for scientific exploration at titan. *Johns Hopkins APL Technical Digest*, 34(3), 374–387.
- Lunine, J. (1997). Titan surface-atmosphere interactions. In: Huygens: Science, Payload and Mission, Proceedings of an ESA conference. Edited by A. Wilson (1997) (p 211).
- Mortari, D., & Wilkins, M. P. (2008). Flower constellation set theory. Part I: Compatibility and phasing. *IEEE Transactions on Aerospace and Electronic Systems*, 44(3), 953–962.
- Mortari, D., Wilkins, M. P., & Bruccoli, C. (2004). The flower constellations. *The Journal of the Astronautical Sciences*, 52, 107–127.
- Nadoushan, M. J., & Assadian, N. (2015). Repeat ground track orbit design with desired revisit time and optimal tilt. *Aerospace Science and Technology*, 40, 200–208.
- Ovchinnikov, M., Shirobokov, M., & Trofimov, S. (2024). Lunar satellite constellations in frozen low orbits. *Aerospace*, 11(11), 1–25.
- Peter, J. S., Nordheim, T. A., & Hand, K. P. (2024). Detection of HCN and diverse redox chemistry in the plume of Enceladus. *Nature Astronomy*, 8(2), 164–173.
- Poggiali, V., Brighi, G., Hayes, A. G., Nicholson, P. D., MacKenzie, S., Lalic, D. E., Bonnefoy, L. E., Oudrhiri, K., Lorenz, R. D., Soderblom, J. M., & Tortora, P. (2024). Surface properties of the seas of Titan as revealed by Cassini mission bistatic radar experiments. *Nature Communications*, 15(1), 1–25.
- Pontani, M., Pustorino, M., & Teofilatto, P. (2022). Mars constellation design and low-thrust deployment using nonlinear orbit control. *The Journal of the Astronautical Sciences*, 69(6), 1691–1725.
- Rianço-Silva, R., Machado, P., Martins, Z., Lellouch, E., Loison, J. C., Dobrijevic, M., Dias, J. A., & Ribeiro, J. (2024). A study of very high resolution visible spectra of Titan: Line characterisation in visible CH4 bands and the search for C3. *Planetary and Space Science*, 240, 1–25.
- Santos, P., Carvalho, J., Vilhena de Moraes, R., & Prado, A. F. B. A. (2013). Dynamics of artificial satellites around Europa. *Mathematical Problems in Engineering*, 2013(1), 1–7.
- Tresaco, E., Elpe, A., & Carvalho, J. P. S. (2016). Frozen orbits for a solar sail around mercury. *Journal of Guidance, Control, and Dynamics*, 39(7), 1659–1666.
- Tresaco, E., Carvalho, J. P. S., Prado, A. F., Elpe, A., & de Moraes, R. V. (2018). Averaged model to study long-term dynamics of a probe about mercury. *Celestial Mechanics and Dynamical Astronomy*, 130(2), 1–25.
- Turtle, E., Perry, J., Barbara, J., Genio, A. D., Rodriguez, S., Mouéllic, S., Sotin, C., Lora, J. M., Faulk, S., Corlies, P., & Kelland, J. (2018). Titan's meteorology over the Cassini mission: Evidence for extensive subsurface methane reservoirs. *Geophysical Research Letters*, 45(11), 5320–5328.
- Vallado, D. (2001). Fundamentals of astrodynamics and applications. Space Technology Library, Microcosm Press.
- Waite, J., Bell, J., Lorenz, R., Achterberg, R., & Flasar, F. M. (2013). A model of variability in Titan's atmospheric structure. *Planetary and Space Science*, 86, 45–56.
- Walker, J. G. (1984). Satellite constellations. *Journal of The British Interplanetary Society*, 37, 559.
- Wertz, J. (2002). Mission geometry; orbit and constellation design and management: Spacecraft orbit and attitude systems. Space Technology Library, (Vol. 13). Microcosm Press.
- Wye, L. C., Zebker, H. A., Ostro, S. J., West, R. D., Gim, Y., & Lorenz, R. D. (2007). Electrical properties of Titan's surface from Cassini RADAR scatterometer measurements. *Icarus*, 188(2), 367–385.



Yang, Y., & Song, X. (2025). Stepwise autonomous orbit determination of large LEO constellations by GNSS observations with partial inter-satellite ranging. *Satellite Navigation*, 6(1), 1-25.

### **Publisher's Note**

Springer Nature remains neutral with regard to jurisdictional claims in published maps and institutional affiliations.